SINGLE AND DOUBLE-LAYER CIRCULAR MICROSTRIP PATCH REFLECTARRAYS

NG WAI HAU

A project report submitted in partial fulfilment of the requirements for the award of Bachelor of Engineering (Hons.) Electronic and Communications Engineering

Faculty of Engineering and Science
Universiti Tunku Abdul Rahman

April 2014

DECLARATION

I hereby declare that this project report is based on my original work except for citations and quotations which have been duly acknowledged. I also declare that it has not been previously and concurrently submitted for any other degree or award at UTAR or other institutions.

Signature : _____

Name : NG WAI HAU

ID No. : 10UEB00022

Date : 14 APRIL 2014

APPROVAL FOR SUBMISSION

I certify that this project report entitled **"SINGLE AND DOUBLE-LAYER CIRCULAR MICROSTRIP PATCH REFLECTARRAYS"** was prepared by **NG WAI HAU** has met the required standard for submission in partial fulfilment of the requirements for the award of Bachelor of Engineering (Hons.) Electronic and Communications Engineering at Universiti Tunku Abdul Rahman.

Approved by,

Signature : _____

Supervisor : DR. LIM ENG HOCK

Date : 14 APRIL 2014

Specially dedicated to
my beloved parents and friends

ACKNOWLEDGEMENTS

First of all, I would like to express my utmost thanks to my supervisor, Dr. Lim Eng Hock for guiding and assisting me throughout my final year project in Universiti Tunku Abdul Rahman. His proper guidance and support have contributed to the completion of this project.

In addition, I would like to express my gratitude to my seniors and friends specifically Wong Hong Yik and Chew Hoo Beng who have helped me in the final year project. They have provided useful information and were willing to lend me a hand whenever I encountered problems. The knowledge that I gained from them is invaluable.

Finally, I would like to express my appreciation to Shin Rou and my family for supporting and motivating me throughout my final year project.

SINGLE AND DOUBLE-LAYER CIRCULAR MICROSTRIP PATCH REFLECTARRAYS

ABSTRACT

A circular microstrip patch centrally etched with a cross slot is studied in the first project. The slot dimensions are varied for controlling the reflection loss and the phase range of a reflectarray. It is found that the dominant TM mode of the slotted circular patch can be easily excited and the slot length can be varied to function as a phase-changing parameter. Cross slots with equal and unequal arms are investigated. Study shows that the slope of the S curve can be made slow-changing by increasing the slot width. A maximum reflection phase range of 328.68º is achievable in the S curve. Rectangular waveguide method has been deployed for simulating and verifying the design idea. Reasonable agreement is found between the measurement and simulation.

In the second project, a microstrip double-layered reflectarray element is studied. The unit element consists of a circular patch which is sandwiched in between two substrates and a cross-slotted circular patch is placed on the top-most surface. The radius of the two circular patches as well as the cross-slot lengths are varied simultaneously for controlling the reflection phase range and the gradient of the S curve. Study shows that the sensitivity of the S curve can be made slower by utilizing substrates with lower dielectric constants. The component was studied using a rectangular waveguide and good agreement is found between the simulation and experiment. A wide reflection phase range of 681.82° with loss magnitude of less than -1 dB is achievable in the S curve. A complete parametric analysis has been conducted to study the reflection characteristics of the proposed reflectarray unit elements.

TABLE OF CONTENTS

LIST OF FIGURES

CHAPTER 1

INTRODUCTION

1.1 Background

Parabolic dish and phase array are the most common antennas used by various wireless applications. By focusing microwave signals into certain directions, both of the parabolic and the phase array antennas are capable to provide high gain. This is much desirable by many wireless applications, particularly, for long-range communications. Parabolic antenna, however, is very bulky because of the focusing dish is typically made of metallic materials (Huang, 1995), making it impractical to be used for space-borne applications where space and weight are crucial. In addition, a mechanical rotator has to be incorporated with a parabolic antenna for enabling multi-direction signal transmission and reception, making it inconvenient. Also, the curvature surface of the parabolic antenna has made the manufacturing process rather difficult and expensive (Zhou et al., 2013). Phase array antenna, as the name implies, is constructed by cascading many antennas with different input phases into array form, which can be a solution to overcome the shortcomings of the parabolic antenna as it allows beam scanning. However, a dedicated power divider is required to provide different phases for each of the individual antennas which in turn cause higher loss to the phase array antenna.

In 1963, Berry et al. introduced the first prototype for reflectarray antenna (Berry, Malech and Kennedy, 1963) which has incorporated the features of the parabolic and the phase array antennas (Mener et al., 2013) while having some of their disadvantages overcome (Mussetta et al., 2007). Reflectarray antenna has a flat

reflecting surface which makes it easy to fabricate as compared to the parabolic reflector (Huang, 1996). Furthermore, it is light in weight and smaller in size, making it suitable to be used for space-borne applications. Unlike phase array antenna, in contrast, a reflectarray antenna does not need a power dividing network to supply different phases to each of its individual elements (Pan, Zhang and Karimkashi, 2012). Each individual element itself is actually a phase shifter which will provide different phases when it is excited by a feed antenna. The antenna gain of the reflectarray antenna can be simply adjusted by varying the number of elements of the antenna.

1.2 Working Principle of the Reflectarray Antenna

When a feed antenna, which functions as microwave source, illuminates electromagnetic waves (EM) on a planar metallic plate, referring to Figure 1.1, the plate reflects the EM waves to some particular directions which can be calculated using Snell's law. Since each of the rays from the feed antenna has a different path length, the reflected waves will not form a coherent wave front. Reflectarray can be easily designed from the reflector structure shown in Figure 1.1, with the plate replaced by arrays of planar resonators so that a coherent wave front can be formed before the aperture.

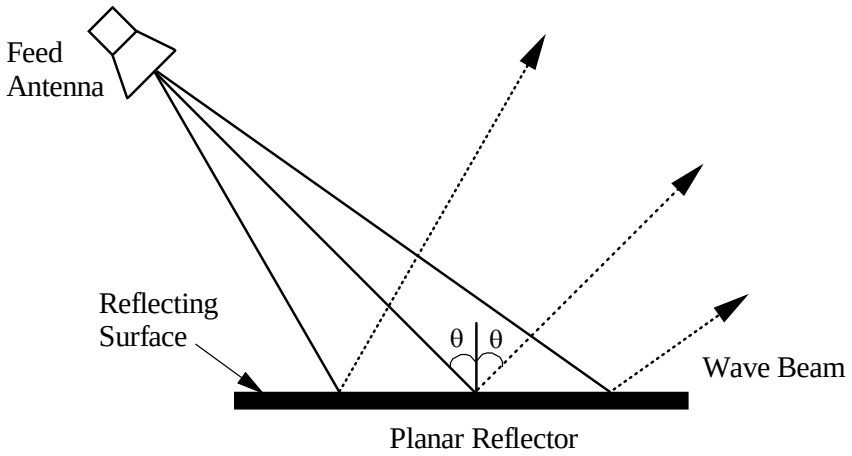

Figure 1.1: A Simple Reflecting Metal Plate.

A simple reflectarray antenna consists of two main components - a feed antenna and a reflecting surface, which is a planar reflector, as depicted in Figure 1.2. The feed antenna is usually placed at an inclination angle (larger than 0°) to avoid blockage of the reflected wave by the feed antenna itself (Han, Huang and Chang, 2006; Mussetta et al., 2006; Yang et al., 2007; Yu, Yang, Elsherbeni and Huang, 2009; Abd-Elhady and Hong, 2010; Budhu and Rahmat-Samii, 2011; Abd-Elhady, Hong and Zhang, 2012), which can significantly affect the performance of the reflectarray antenna. In order to compensate the phase differences in the reflected waves, the metallic planar reflector is replaced with a grounded substrate with a series of top-loading radiating elements shown in Figure 1.2. The radiating elements absorb the incoming waves from the feed antenna, resonate and finally reradiate the waves in the direction normal to them. A certain phase shift is introduced by each of the radiating elements to the incoming waves such that all of the wave beams are reflected in a coherent manner with equal wave front along the line *O – O'* (Zhang, Fu and Wang, 2007). The most common way for generating phase shift in each radiating element is to alter its geometrical design parameters.

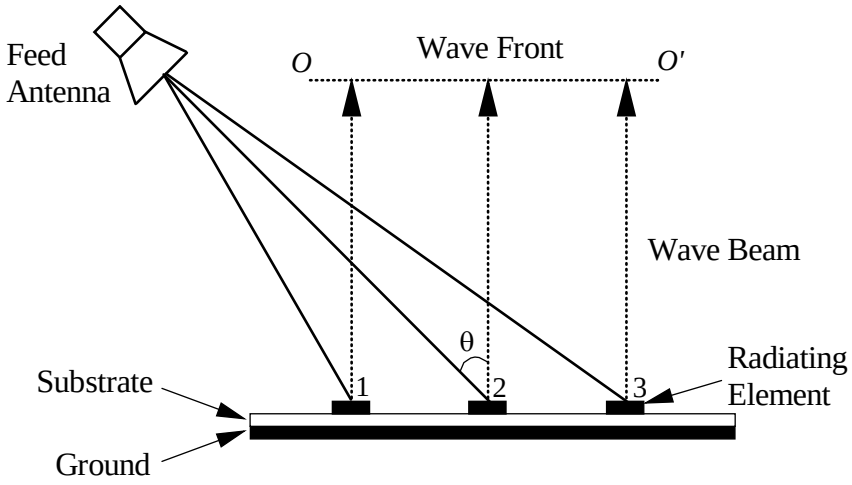

Figure 1.2: A Reflectarray Antenna Consisting of Radiating Elements Placed on a Grounded Substrate.

1.3 Unit Element Key Performance Parameters

As explained in the previous section, the main purpose of having unit elements in the reflectarray antenna is to introduce phase shifts to the incoming wave so that the reflected wave beams will be all in phase. The performance of the reflectarray antenna is therefore closely related to the reflection characteristics of the unit elements. It is necessary to optimize the reflection characteristics of the unit elements in order to produce a good-performing reflectarray antenna. In this section, the main performance parameters of the unit element will be discussed.

1.3.1 Reflection Loss

In the process of absorbing, resonating, and reradiating the incoming wave from the feed antenna, a reflectarray unit element dissipates energy in two forms of losses - metallic ohmic loss and dielectric loss (Bozzi, Germani and Perregrini, 2004). Metallic ohmic loss refers to the loss caused by any metal that exists in the unit element while dielectric loss refers to the loss induced by the substrate of the unit element. In other words, the energy of the incoming wave is partially absorbed by the metal and substrate of the unit element and then dissipated as heat.

It was reported by (Rajagopalan and Rahmat-Samii, 2010) that the loss tangent and the thickness of a substrate have great effects on the reflection characteristics. Thicker substrate exhibits lower reflection loss (Karnati, Yusuf, Ebadi and Gong, 2013). The shape of the unit element is also one of the factors that affects the amount of reflection loss (Bozzi, Germani and Perregrini, 2004). In the unit element simulation, the reflection loss of a unit element is extracted from the magnitude of the reflection coefficient (S_{11}) at a certain frequency. Minimum reflection loss is much desired in designing the unit element so that higher radiation efficiency can be achieved for a reflectarray antenna.

1.3.2 Reflection Phase

Reflection phase is another important parameter that needs to be considered in designing the unit element. It is also known as S curve. The S curve of the unit element is extracted from the phase of the reflection coefficient (S_{11}) at a certain frequency in the unit element simulation. It represents the relationship between the reflection phase and a particular phase-changing design parameter, for example, it can be the patch size, substrate thickness or dielectric properties of the unit element.

In the S curve, there are two things that need to be considered - the phase range and the phase slope. When designing a unit element, a phase range of larger than 360° is always desirable as it can be used to design reflectarrays of any sizes. Phase slope describes the sensitivity of the reflection phase with respect to the variation of the phase-changing design parameter. A slower curve gradient is always desired to make the unit elements more distinguishable in dimension. It was explained in (Hasani, Kamyab and Mirkamali, 2010) that a slow changing rate of S curve can be achieved by using a thicker substrate. Other methods of achieving slower gradient include the use of phase-delay lines (Carrasco, Arrebola and Encinar, 2007) and stacked patches (Encinar, 1999, 2001).

1.4 Reflectarray Key Performance Parameters

Reflectarray is a type of antenna which consists of many unit elements arranged in array form, with the neighbouring elements having equal/unequal separation distances. Each element is responsible to convert the spherical wave front of the incoming wave~~,~~ emitted from the feed horn, into a planar wave front (Bialkowski and Sayidmarie, 2008). A directive radiation beam can be formed when the reflected wave rays are all in phase (Karnati et al., 2013). There are two main parameters which can be used to evaluate the performance of the reflectarray and they will be discussed in the following subsections.

1.4.1 Antenna Gain

Antenna gain refers to the ability of an antenna to direct electromagnetic waves in a particular direction. It is usually measured in dBi (the gain of the reflectarray with respect to the gain of isotropic radiator). The gain of the reflectarray is mainly affected by the size of the aperture (Huang and Encinar, 2007). Larger size of reflectarray will be able to provide higher antenna gain. The feeding angle of the feed horn will also affect the reflectarray gain. It is recommended that the feed horn to be placed at an angle larger than 0° to avoid scattering of the reflected waves caused by the feed horn, which will significantly reduce the gain of the reflectarray. The spill-over loss is another factor that affects the reflectarray gain. This loss can be mitigated by placing the feed horn nearer to the reflectarray, but maintaining far-field distance between the feed horn and all of the reflectarray elements.

1.4.2 Gain Bandwidth

Gain bandwidth refers to the range of frequencies at which the gain of the reflectarray drops by 1 dB. It is the bandwidth of the unit element that limits the gain bandwidth of the reflectarray (Huang and Encinar, 2007). Microstrip reflectarray is well known to have narrow bandwidth performance. However, with the use of thicker substrate and stacked patches, the bandwidth of a microstrip reflectarray can be improved (Encinar, 1999; Encinar and Zornoza, 2003).

1.5 Aims and Objectives

The original aim of this thesis was to design two novel microstrip-based reflectarrays. However, due to time restriction, the aim of the thesis has been changed to analysing two unique microstrip-based unit elements. This thesis can be divided into two parts. In the first part, a single-layer structure is explored for designing the microstrip reflectarray element. Later, by adding an additional layer to the single-layer structure,

a double-layer reflectarray element has been explored for broad range performance. The commercial software, CST Microwave Studio, was used to design and simulate the proposed unit elements. Experiment was also conducted using the waveguide method to verify the simulation results. The details will be further explained in the following paragraphs.

In Chapter 3, for the first time, a single-layer cross-slotted circular patch unit element which operates at 6.5 GHz is designed. The lengths of the slots are varied simultaneously to provide phase shifts to the S curve. It has been found that a reflection phase range of 328.68° is obtainable. Experiment has been performed to verify the simulation results. A complete parametric analysis has been conducted to study the reflection characteristics of the proposed reflectarray unit element.

In Chapter 4, again for the first time, a novel double-layer circular microstrip unit element is designed. It is an expansion of the work in Chapter 3 by adding another resonator beneath the original structure. The new structure consists of a top-loading circular patch centrally etched with a cross slot and a circular patch in the middle. To provide phase shift, the slot lengths are varied as a function of the patch radii. A gradual decreasing phase slope with a total reflection phase range of 681.82° is achievable. Again, the simulation results are verified by the experiments. Parametric analysis has also been conducted to visualize the effects of the physical design parameters on the reflection properties of the proposed double-layer unit element.

1.6 Thesis Overview

In Chapter 1, the contemporary issues and the design concepts of the reflectarray antenna are discussed. Here, the working principle of the reflectarray antenna and the key performance parameters of the unit elements and the reflectarrays are explained. Finally, the aims and objectives of the research are ensued.

Chapter 2 begins with the review of reflectarray antennas, along with a brief introduction of the microstrip reflectarray. The design method of the unit element is then presented, following by a brief description on the design process of a practical reflectarray.

Chapter 3 focuses on the design procedure of a single layer microstrip reflectarray unit element. Details of the unit element structure, along with the simulation and measurement results, are included. A complete parametric analysis has also been conducted to study the reflection characteristics of the proposed unit element.

Chapter 4 presents the design steps of the double-layered microstrip reflectarray unit element. The unit element configuration together with the simulation and experimental results are included. Complete parametric analysis has been presented as well.

Chapter 5 concludes the works completed in this thesis, along with some recommendations for future research.

CHAPTER 2

LITERATURE REVIEW AND DESIGN METHODOLOGY

2.1 Review on Reflectarray Antennas

The concept of reflectarray was first introduced by Berry, Malech, and Kennedy in the early 60s (Berry, Malech and Kennedy, 1963). The first reflectarray was constructed using multiple shorted-end variable-length waveguides cascaded in array. The phases of the radiating waves can be tuned by varying the length of each individual waveguide. In the mid 70s, (Phelan, 1977) came up with an idea of spiraphase reflectarray in which switching diodes were integrated with the four-arm spiral antennas. This technique allows the reflectarray to have a larger beam scanning angle in the broadside direction.

In the late 70s, reflectarray that was designed using the microstrip elements, was first proposed and constructed by (Malagisi, 1978). Since then, various kinds of microstrip elements have been proposed for designing reflectarrays. In (Huang, 1991; Chang and Huang, 1995), the lengths of the phase delay lines, which are attached to the microstrip patches, are varied to provide different phase shifts to the reflectarray elements. In (Pozar and Metzler, 1993; Pozar, Targonski and Syrigos, 1997), microstrip patches with variable patch sizes are used to compensate the phase differences of the reflect waves. Variable-size dipoles (Pozar, Targonski and Pokuls, 1999) and rings (Guo and Barton, 1995) are also some of the alternatives for designing reflectarrays. The recent developments of the microstrip reflectarrays will be further discussed in Chapter 3 and 4.

2.2 Review of Design Methods

There are two methods for designing a reflectarray, namely, the direct optimization technique (DOT) and the phase-only optimization technique (POT). The DOT is only advantageous when arbitrary-shaped array elements without fixed orientations and positions are used to design a reflectarray. An example of reflectarray which is designed using the DOT is shown in (Zhou et al., 2013). Contrary to the DOT, the POT is applied when the unit elements of the reflectarray are arranged in square grid, with the elements having equal/unequal spacings between the adjacent elements. It has better efficiency in terms of computation time as compared to the DOT, making it a more popular choice for designing the reflectarray. This technique has been extensively used in designing various types of reflectarrays as demonstrated in (Encinar and Zornoza, 2004; Carrasco, Arrebola and Encinar, 2007; Carrasco, Arrebola, Encinar and Barba, 2008; Capozzoli et al., 2009; Encinar, Arrebola, Fuente and Toso, 2011). The POT, in general, involves two important steps. The number of unit elements on the reflectarray, which determines the size of the reflectarray, is first determined. The compensating phase shift for each unit element is then calculated by comparing its wave propagation phase to a referencing element (Zhou et al., 2013). The referencing element is usually chosen to be the one which has the shortest propagation path length from the feed horn.

2.3 Design Procedures

In this thesis, the phase-only optimization technique is applied to design the reflectarrays. A brief and concise design procedure is shown in Figure 2.1. The design begins with the simulation of a single unit element with the purpose of obtaining the reflection loss and the S curve of the element. An oblique incident wave is applied when simulating the unit element. At this stage, the physical design parameter of the unit element that is able to provide phase shift is determined and varied to study its effect on the reflection phase. The S curve is then plotted by combining all of the phases for different dimensions.

By knowing the reflection phase range a unit element can provide, the size of the reflectarray is defined. The path lengths for the electromagnetic waves to travel from the feed horn which is placed at the minimum far field distance with a fixed inclination angle to all of the unit elements are then calculated. Subsequently, the propagating phases for all path lengths are determined. By choosing a referencing element, which usually has the shortest path length from the feed horn, the phase shift that is required by a particular unit element can be calculated by finding the phase difference between the referencing element and itself. With the obtained phase difference, the dimension needed by this unit element can then be extracted from the S curve.

Finally, the reflectarray model will be constructed and simulated using the CST Microwave Studio. For actual implementation, a prototype can be fabricated and measured to verify the simulated result. Detailed explanations on the design procedures are shown in Figure 2.1 will be provided in the following sections.

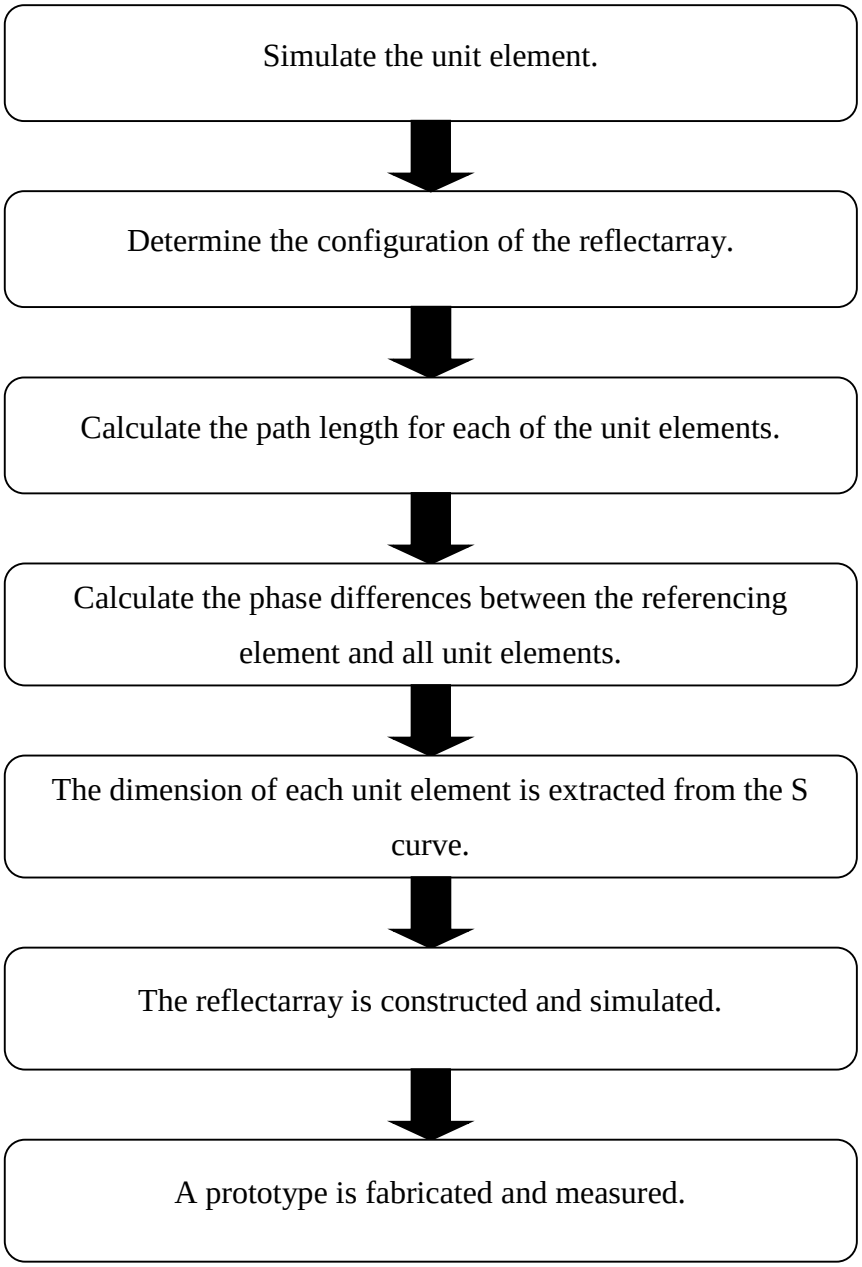

Figure 2.1: Design Process of a Reflectarray Antenna with the Use of the Phase-Only Optimization Technique.

2.4 Simulation of Unit Element

The main purpose of simulating a unit element is to study its reflection characteristics. It is very important to identify a particular physical design parameter that is capable of providing low reflection loss and broad phase range. There are two common methods which can be used to simulate the unit element, namely, the waveguide method and the Floquet method.

2.4.1 Waveguide Method

The waveguide method has boundary conditions with all four walls defined as perfect electrical conductor (PEC) as illustrated in Figure 2.2. In the waveguide method, the unit element is placed at one end of the waveguide section and it is excited by the electromagnetic waves generated at another end of the waveguide section, which is the waveguide port. The illuminating angle (α) of the electromagnetic waves changes with respect to the operating frequency and the waveguide cut-off frequency. It can be calculated using equation (2.1).

$$\sim = 90° - \cos^{-1}\sqrt{1-\left(\frac{f_c}{f}\right)^2} \tag{2.1}$$

where

α = illuminating angle of the electromagnetic waves (°)

f_c = waveguide cut-off frequency, Hz

f = operating frequency, Hz

The main disadvantage of the waveguide method is that the size of the unit element dimension is restricted by the waveguide dimension ($a \times b$), making this method unsuitable for simulating a unit element that has dimension larger than the waveguide cross section.

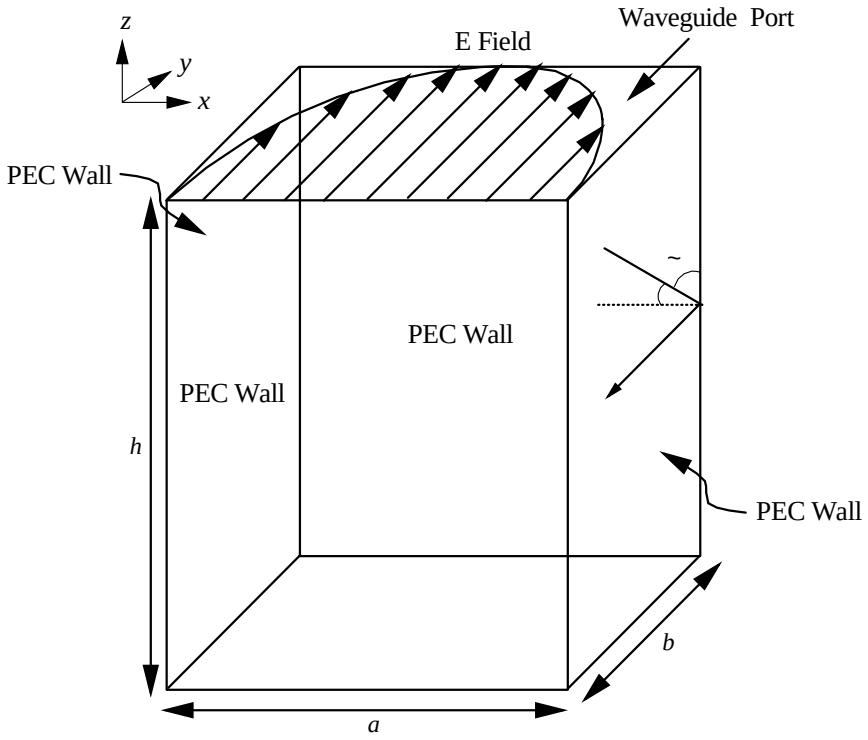

Figure 2.2: Boundary Conditions of the Waveguide Method.

2.4.2 Floquet Method

The Floquet method has different boundary conditions. Two of its boundaries are defined as the perfect electrical conductors (PEC) while the other two to be defined as the perfect magnetic conductors (PMC). It provides a much accurate unit element simulation by considering the mutual coupling from the neighbouring elements (Dzulkipli et al., 2012). Unlike the waveguide method, Floquet method can be used to simulate any unit elements regardless of their sizes. Since the illuminating angle for the Floquet method is not restricted by the operating frequency, it gives much more freedom in choosing the operating frequency and the illuminating angle when designing a unit element. In other words, l_1 and l_2 can be made any values. The disadvantage of the Floquet method is that a unit element that is simulated using this method cannot be verified experimentally.

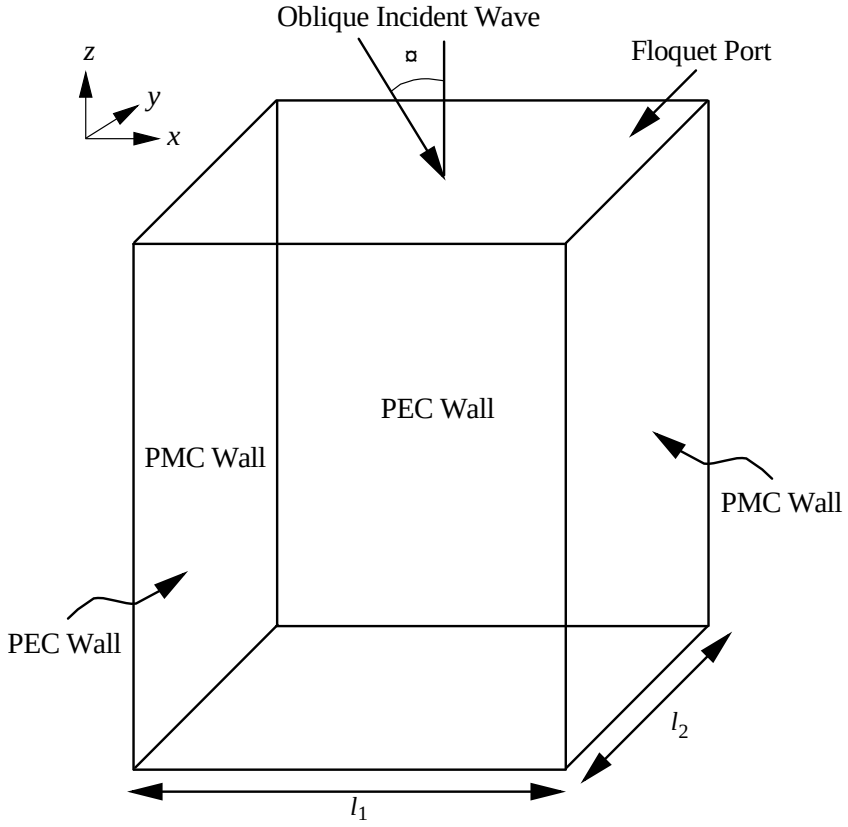

Figure 2.3: Boundary Conditions of the Floquet Method.

2.5 Configuration of Reflectarray

The size of a reflectarray and the position of the feed horn are among the most important things that have to be considered before the reflectarray can be designed. The side view of the reflectarray is depicted in Figure 2.4. The number of unit elements which is corresponding to the size of the reflectarray will determine the gain of the reflectarray. More unit elements on the reflectarray will contribute to a higher antenna gain. The gain of the reflectarray can be further improved by introducing suitable spacing between unit elements. The feed horn is placed at a focal distance *f* away from the middle point of the reflectarray radiation aperture and it must be kept at a far field distance from all of the unit elements. Centre-fed ($\theta = 0°$) or side-fed ($\theta > 0°$) feeding schemes can be used. To maximize the performance of the reflectarray, the side-fed configuration is usually used as it can avoid blockage of the reflected waves by the feed horn. The focal distance *f* and the aperture dimension

(*D*) of the reflectarray are interrelated. They are expressed in the ratio of *f/D* which has a typical value of 1 (Zhao et al., 2013).

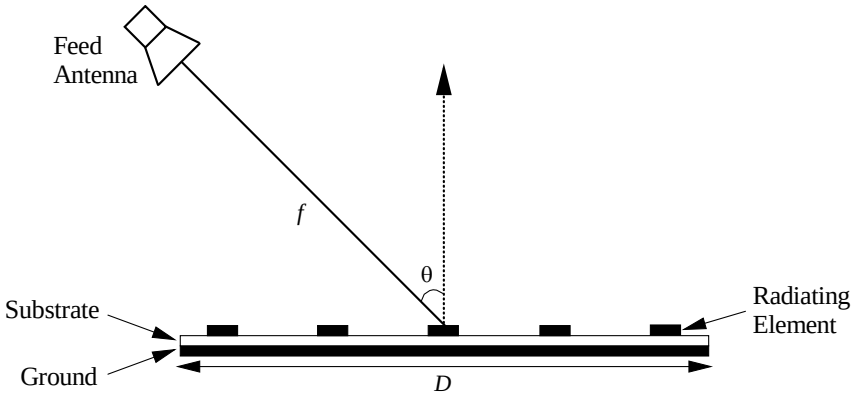

Figure 2.4: Configuration of a Reflectarray.

2.6 Calculation of Path Length

The paths (d_1, d_2, d_3, …, d_n) for electromagnetic waves to propagate from the feed horn to the unit elements are illustrated in Figure 2.5. Since the unit elements are located at different distances from the feed horn, the lengths of their propagation paths are also different ($d_1 \neq d_2 \neq d_3 \ldots \neq d_n$). The propagation path lengths for all the unit elements from the feed horn can be easily calculated from the locations of the elements.

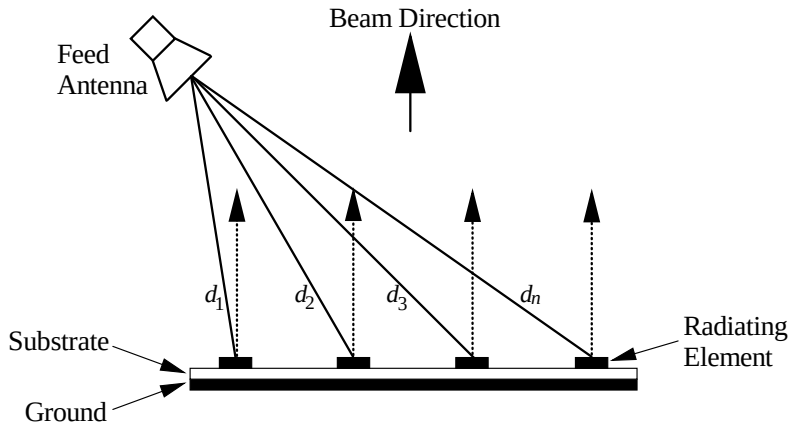

Figure 2.5: Propagating Path Lengths of All the Unit Elements from the Feed Horn.

2.7 Calculation of Phase Difference

After knowing the path lengths, the propagation phases for all the unit elements can be calculated using the formula shown in equation (2.2).

$$\theta_n = \frac{2\pi}{\lambda_o}(d_n) \tag{2.2}$$

where

θ_n = propagating phase for the n-th element, rad

d_n = path length for the n-th element, m

λ_o = wavelength at the operating frequency of the reflectarray, m

With the propagation phases of all the unit elements calculated, the phase shift requires by each of the unit elements can then be determined. This can be easily done by first selecting the referencing element, and then, finding the phase difference between the referencing element and a particular unit element. For ease of calculation, the referencing element is usually chosen to be the one which has the shortest propagation path length from the feed horn, for example, in this case is d_1. The additional phase shifts introduced by the unit elements will make the reflected wave beams to be in-phase.

2.8 Extraction of Dimension from S curve

The dimension of a particular unit element can then be extracted from the S curve after finding out the phase difference between the referencing element and this unit element itself.

2.9 Simulation of Reflectarray

At the final stage, the reflectarray model is constructed using the CST Microwave Studio. A feed horn is constructed and simulated together with the reflectarray. The radiation patterns of the reflectarray can then be obtained. By inspecting the resulting radiation patterns, the performance of the reflectarray can be easily validated.

CHAPTER 3

STUDY OF CROSS-SLOTTED CIRCULAR MICROSTRIP FOR REFLECTARRAY DESIGN

3.1 Introduction

Reflectarray antenna was first proposed by Berry et al. in 1963 (Berry, Malech and Kennedy, 1963) with the intention of providing a better solution than the parabolic reflector and phased array. Although containing both features, its implementation using truncated waveguides made it extremely bulky. This problem was later solved with the introduction of microstrip reflectarray (Pozar, Targonski and Syrigos, 1997; Huang and Encinar, 2007) in 1991, which provided advantages such as low profile, flat surface, and low manufacturing costs. A microstrip reflectarray consists of an array of microstrip resonators, also known as unit elements, printed on a grounded substrate. A good unit element should possess low reflection loss, slow reflection phase change, and large reflection phase range. Additional reflection phase can also be easily introduced by changing of resonator size (Encinar, 2001) or by loading a microstrip patch with an additional phase-delay stubs (Huang, 1995) for linear polarization.

Microstrip patch is the earliest planar resonator explored for designing various reflectarrays due to its simplicity. Loading patch with slots was found to be able to provide phase shifts that are required for designing a reflectarray (Trampuz, Hajian and Ligthart, 2006; Cadoret, Laisné, Gillard and Legay, 2005). This method is very easy in the sense that the separation distance between any two of the elements is a constant. In (Trampuz, Hajian and Ligthart, 2006), it was shown that a phase range

of about 270° can be achieved by introducing a square hole in the middle of a rectangular patch. However, the phase range obtained is still less than the optimal phase range of 360° and is insufficient to build a large-size reflectarray. A triple-patch structure loaded with double slots was proven to be able to provide a phase range of greater than 360° (Cadoret et al., 2005), but it has many parameters to be optimized. Multilayer microstrip patch unit element structure is another option that is able to introduce reflection phase shift for designing reflectarray (Chaharmir, Shaker, Cuhaci and Sebak, 2003; Pham et al., 2012). In (Chaharmir et al., 2003), a multilayer unit element with variable slot lengths etched on its ground plane is proven to be able to provide phase range of 330°, however, the gradient of the S curve changes too rapidly, making it difficult to be used as a reflectarray element. An annular slot and a C patch can be combined to design a broad-range reflectarray (Pham et al., 2012). Unfortunately, fine tuning such a multilayer structure may not be easy. Other broad-range configurations such as circular patch, ring (Zhou Danchen, Niu Zhenyi and Li Ruilin, 2011), and fractal-shaped (Zubir and Rahim, 2009) unit elements have also been demonstrated. Adding planar amplifier arrays to a passive microstrip unit element was shown to be another possible way for designing reflectarray (Robinson and Bialkowski, 1997). However, the use of active elements in the design can introduce a higher loss which in turn compromises the radiation efficiency of a reflectarray.

In this chapter, a unit element made of a cross-slotted circular microstrip patch is explored for reflectarray design. The reflection properties are studied for different slot dimensions. It is found that the dimensions of the cross slot can be used to tune the reflection loss and phase range of the patch element. Slots with equal and unequal arms are studied. Simulations were conducted using the CST Microwave Studio software, and experimental verification was done using the R&S®ZVB8 Vector Network Analyzer (VNA). The resonance is analyzed, along with a comprehensive parametric analysis.

3.2 Unit Cell Structure

Figure 3.1 shows the schematic of the proposed unit element which is made of a circular microstrip patch, working at the resonant frequency of 6.5 GHz, with a cross slot etched at its centre. It is made on a Duroid RO4003C substrate with a thickness of 1.524 mm and a dielectric constant of $\varepsilon_r = 3.38$, with its ground laminated on the reverse surface. The circular patch has a radius of R = 5.5 mm. With reference to Figure 3.1 (a), the cross slot is built by intersecting a horizontal (y-directed) slot and a vertical (x-directed) rectangular slot with their widths given by $W_1 = W_2 = 1.4$ mm. Here, the slot lengths (L_1, L_2) are used as the phase-shifting elements. Figure 3.1 (b) shows the fabricated sample. Waveguide method is adopted to characterize the proposed design. A section of C-band waveguide (a = 34.85 mm × b = 15.8 mm, covering 5.8 GHz – 8.2 GHz) with length of 154 mm, is used for measurement.

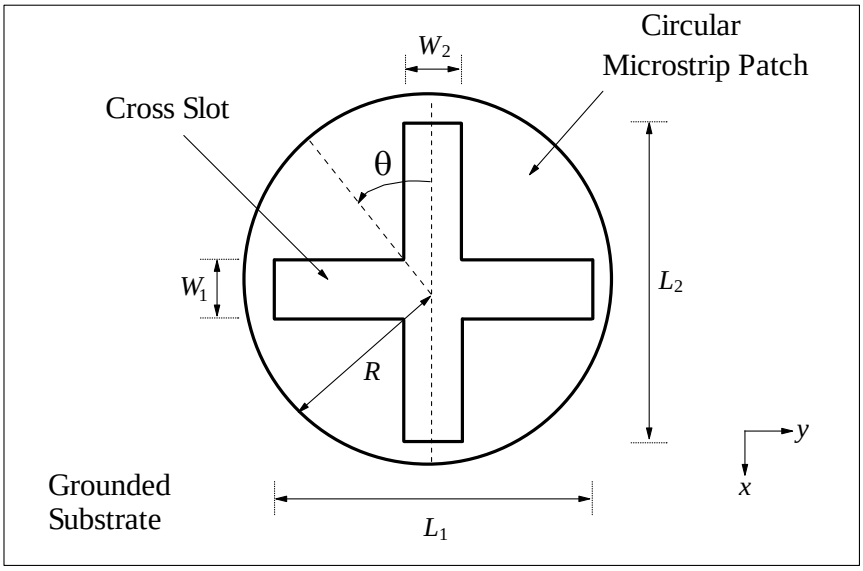

(a)

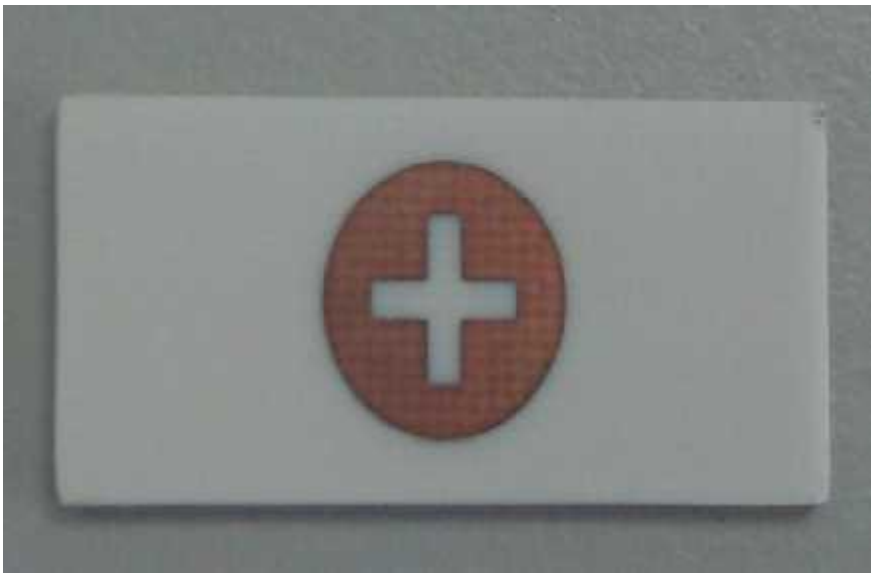

(b)

Figure 3.1: (a) Schematic of the Proposed Circular Microstrip Patch with a Cross Slot at the Centre. (b) Photograph of the Fabricated Sample.

Figure 3.2 (a) shows the measurement setup with its corresponding simulation model depicted in Figure 3.2 (b). It can be seen that the sample is placed inside a rectangular trench carved on a metallic shorting plate, with the patch aligned flush to the metal surface. Electromagnetic wave is guided from the coaxial-to-waveguide adaptor, travelling along the length of the waveguide section to reach the slotted patch, which is placed on the other end. In measurement, the reference plane is de-embedded down to the waveguide flange of the adaptor. An *x*-polarized wave is launched from the wave port, as can be seen from the simulation model in Figure 3.2 (b), with the patch and substrate located on the other end of the waveguide section. All lateral walls are defined to be perfect electric conductors (PEC) in simulation.

(a)

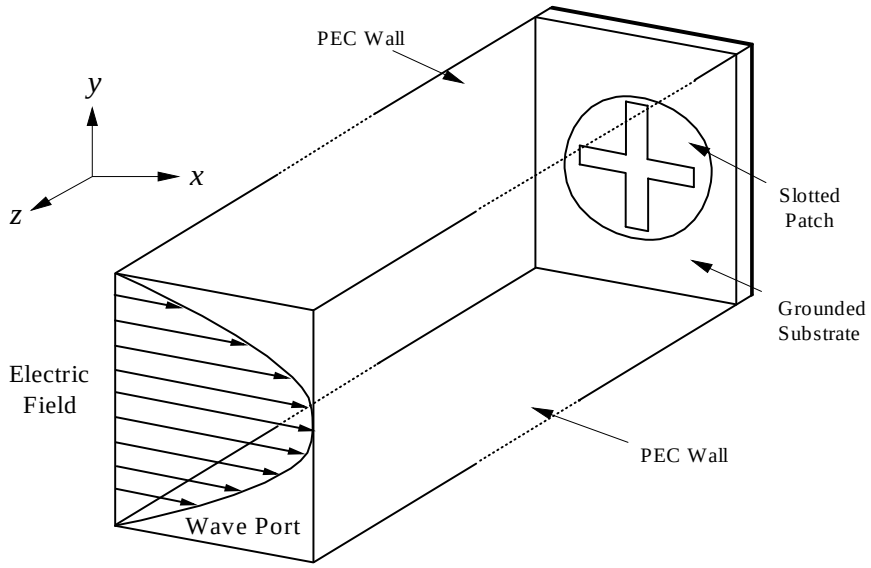

(b)

Figure 3.2: (a) Photograph of the Measurement Setup. (b) Simulation Model for the Proposed Cross-Slotted Circular Patch Unit Cell.

3.3 Electric Field Distributions

The proposed slotted patch is one type of microstrip resonator, with its top and bottom walls defined as good electrical conductor while the side wall delineated as good magnetic conductor. It can be analyzed using the circular patch cavity model (TM^{z}_{mn0}) and is best described using the cylindrical coordinate system (ρ, φ, z), as shown in Figure 3.3.

Figure 3.4 (a) shows the electric field distributions formed in between the cross-slotted circular microstrip patch resonator and its ground when it is excited by an incident wave of 6.5 GHz. For comparison purpose, the electric field for a solid circular patch is also given in Figure 3.4 (b), which can be easily observed to be the dominant mode, TM^{z}_{110} model (Watkins, 1969; Khor, Lim and Chung, 2014).

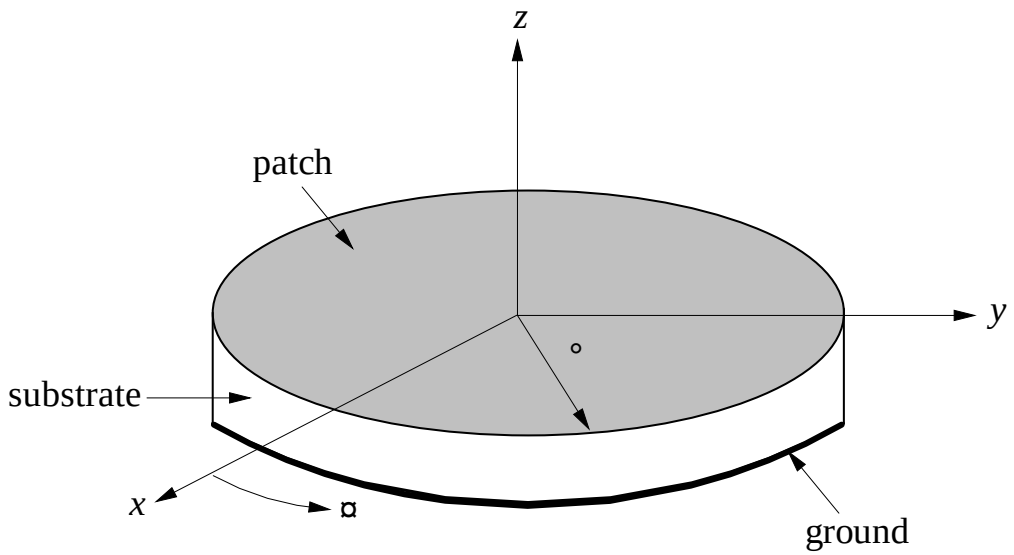

Figure 3.3: Circular Patch Cavity Model.

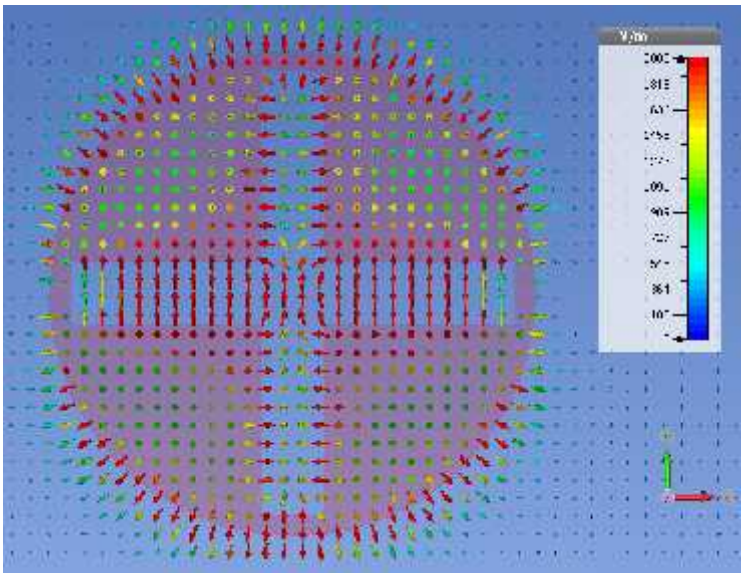

(a)

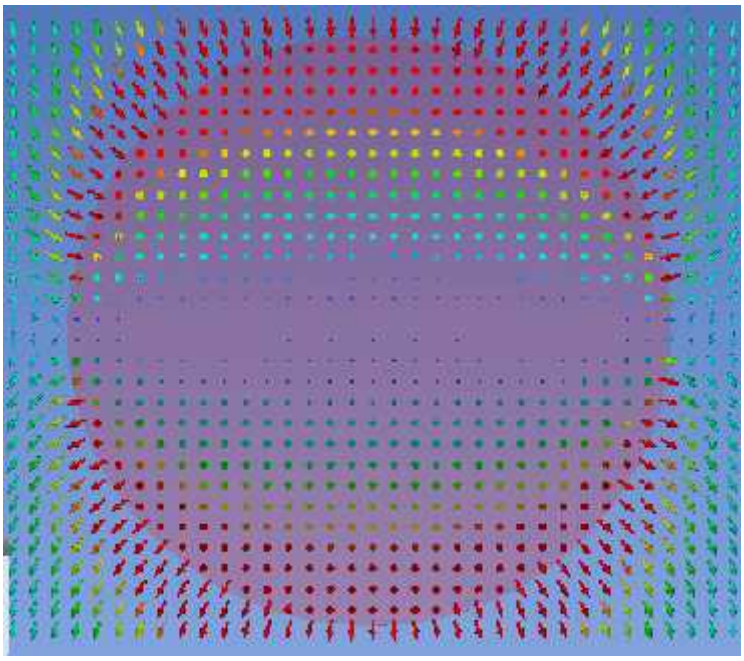

(b)

Figure 3.4: Electric Field Distributions on the Circular Patch (a) with Cross Slot (*R* = 5.5 mm, L_1 = L_2 = 10 mm, and W_1 = W_2 = 1.4 mm), (b) without Cross Slot.

3.4 Unit Cell Simulation and Measurement Results

Figure 3.5 depicts the simulated and measured reflection losses and reflection phases (S curves) of the proposed unit element when both of the slot lengths (L_1, L_2) are varied simultaneously. Generally, the measurement result agrees reasonably well with simulation. Referring to Figure 3.5 (a), the measured reflection loss peaks at -1 dB at the slot length of 6.5 mm while the simulated reflection loss peaks at -1.3 dB at the slot length of 7.5 mm. Low reflection loss implies that the unit element dissipates very little power for all dimensions of the cross slot. Figure 3.5 (b) shows the simulated and measured S curves. A gradual decreasing slope with a total reflection phase range of 328.68º is successfully achieved. This phase range is sufficient for designing small-size reflectarrays.

Figure 3.6 depicts the simulated and measured frequency responses for the case of $L_1 = L_2 = 9.5$ mm in the range 6.3 GHz - 6.7 GHz. Reasonable agreement is found between the simulated and measured results. With reference to Figure 3.6 (a), the measured reflection has the same trend with its simulation, both are increasing with frequency. Higher loss (~ 0.3 dB) is observed in the measurement due to minor impedance mismatch which is unavoidable. With reference to Figure 3.6 (b), minor discrepancy (~1%) is found between the measured and simulated reflection phases, which is acceptable.

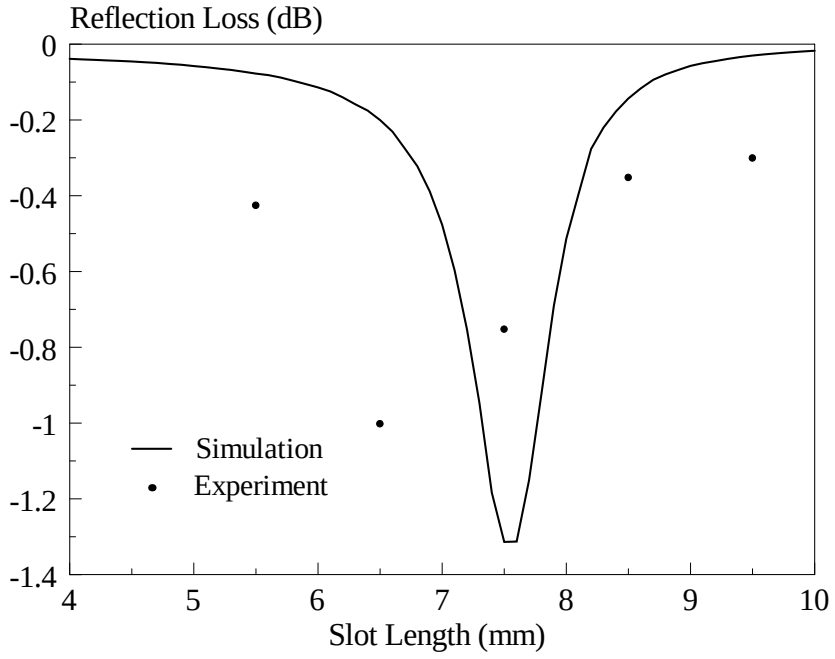

(a)

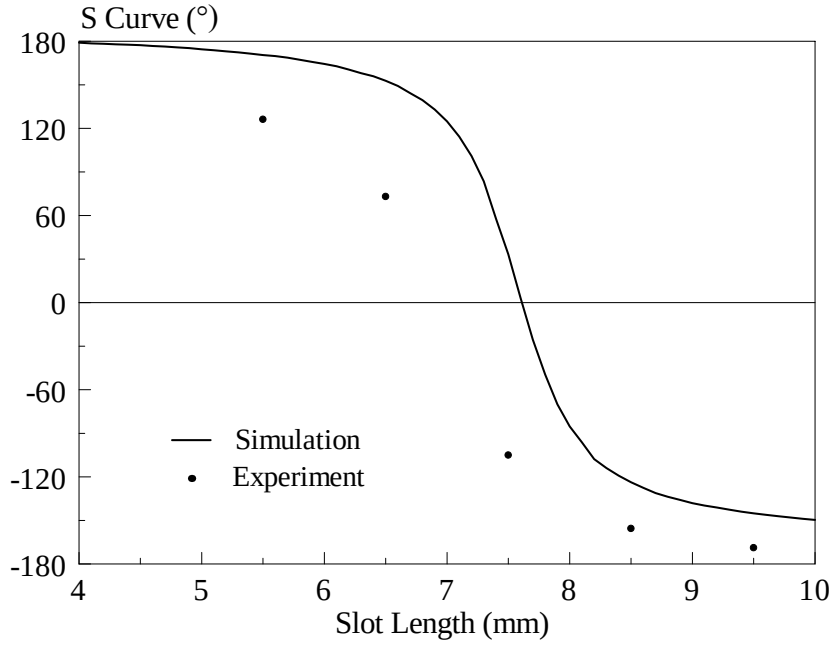

(b)

Figure 3.5: Measured and Simulated (a) Reflection Losses; (b) S Curves of the Proposed Cross-Slotted Circular Patch Unit Cell.

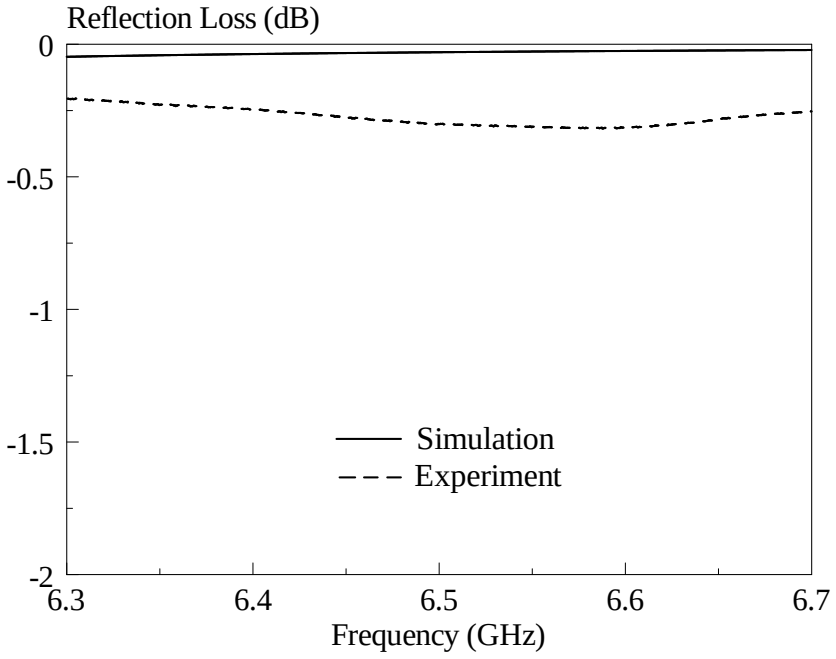

(a)

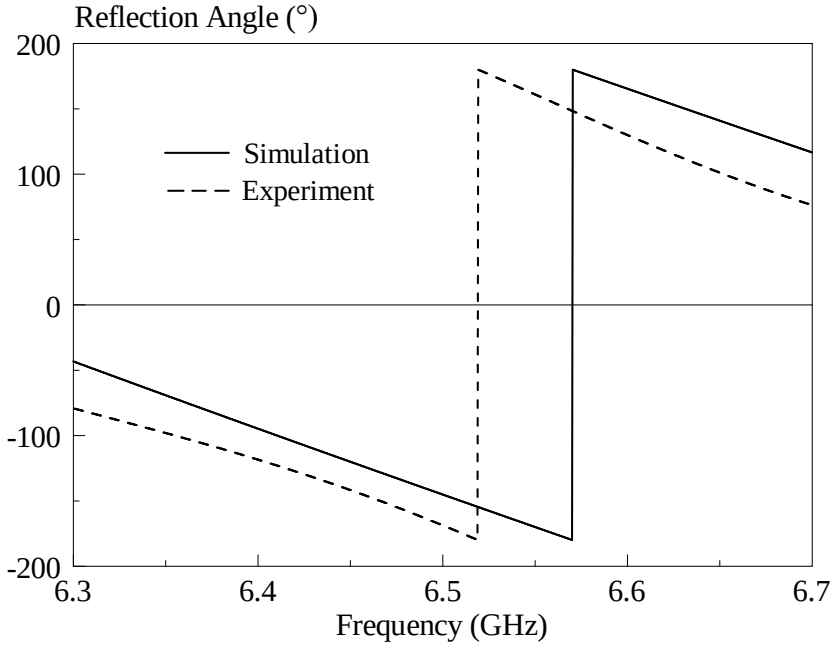

(b)

Figure 3.6: Measured and Simulated (a) Reflection Losses; (b) Reflection Angles against Frequency for $L_1 = L_2 = 9.5$ mm for the Proposed Cross-Slotted Circular Patch Unit Cell.

3.5 Parametric Analysis

Parametric analysis has been conducted to visualize the effects of the key design parameters on the reflection loss and the S curve of the proposed cross-slotted circular patch unit element. The reflection performances of the cross-slotted circular and the cross-slotted square patch are also compared.

3.5.1 Slot Length

The reflection characteristics of the proposed unit element are first studied by varying the horizontal slot length (L_1). With reference to Figure 3.7, it can be observed that adjusting the length of the horizontal (L_1) slot has no impact on the reflection performance at all when the vertical slot length (L_2) is varied from 4 to 10 mm. The vertical slot length (L_2) is now studied, with its horizontal slot length (L_1) swept from 2 to 10 mm. It was found that changing slot length L_2 does not affect the reflection characteristics of the slotted patch much, as can be seen from Figure 3.8.

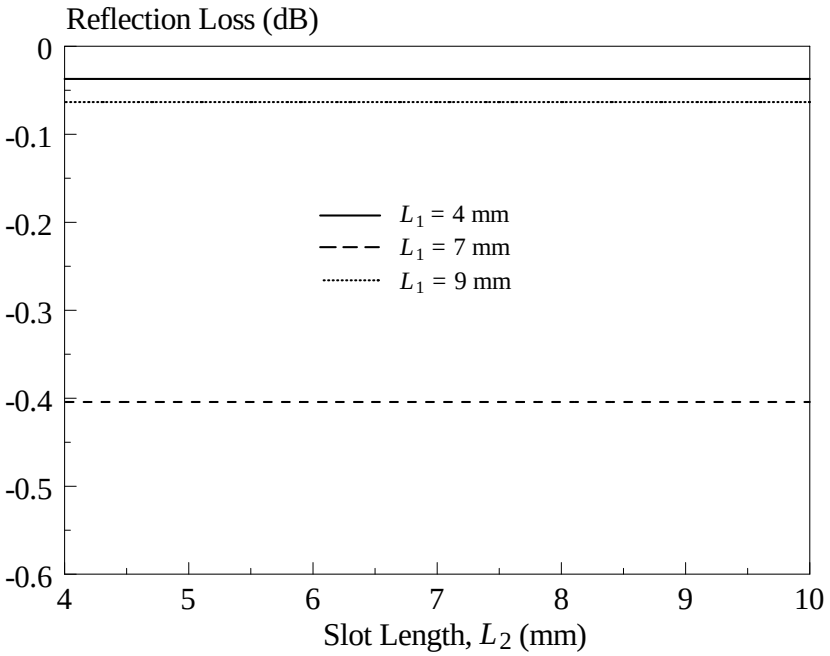

(a)

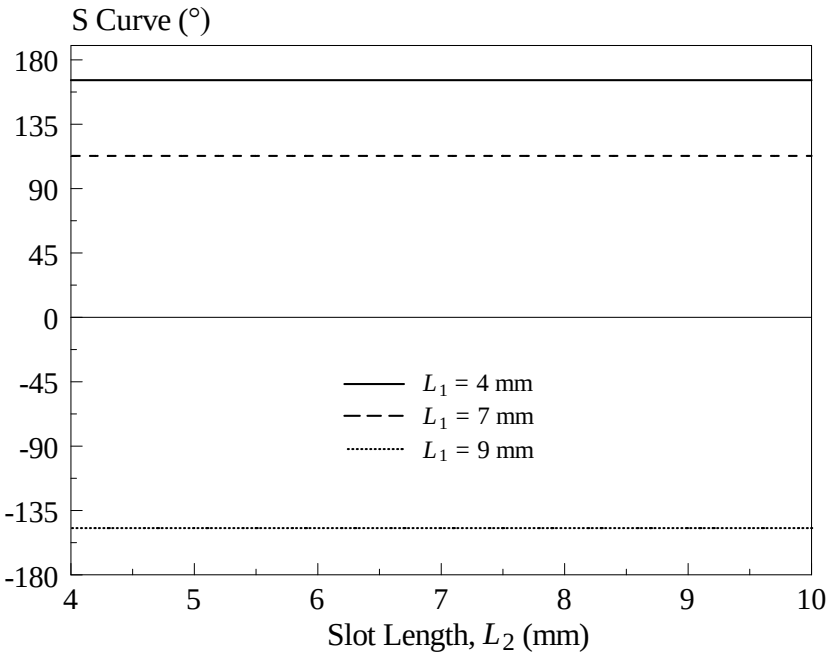

(b)

Figure 3.7: Effects of the Horizontal Slot Length L_1 on the (a) Reflection Loss; (b) S Curve of the Proposed Cross-Slotted Circular Patch Reflectarray Unit Cell.

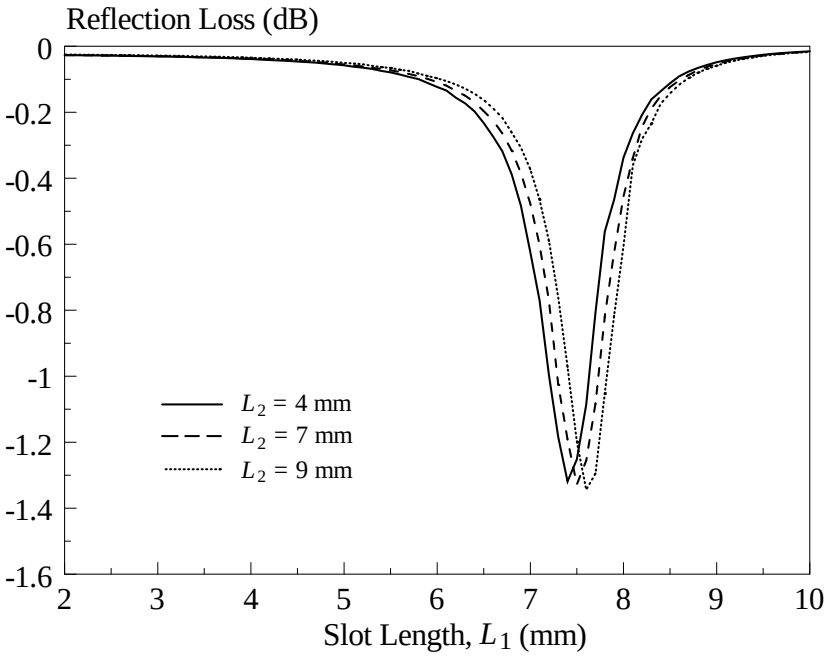

(a)

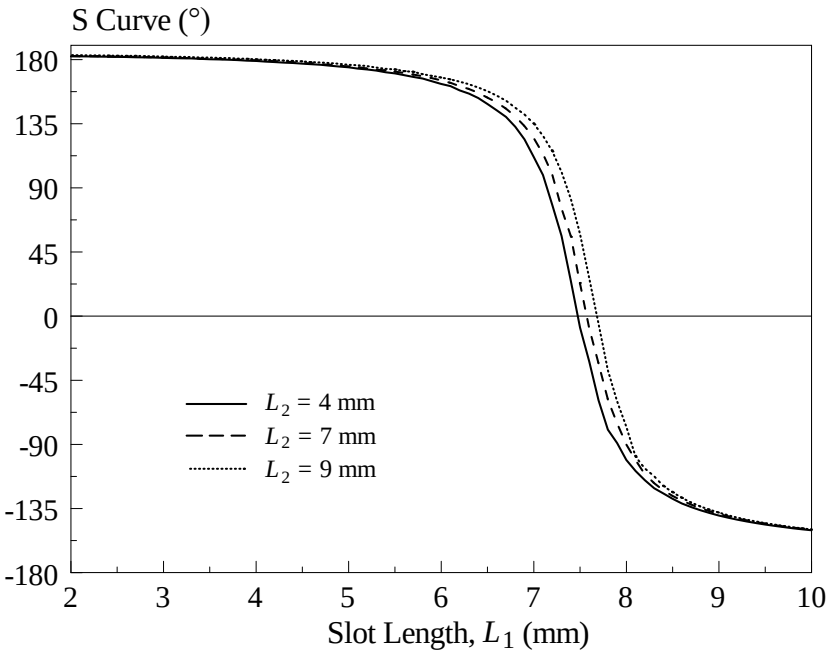

(b)

Figure 3.8: Effects of the Vertical Slot Length L_2 on the (a) Reflection Loss; (b) S Curve of the Proposed Cross-Slotted Circular Patch Reflectarray Unit Cell.

3.5.2 Slot Width

The effects of the slot widths (W_1, W_2) are studied first. With reference to Figure 3.9, the lengths of the horizontal (L_1) and vertical (L_2) slots are varied simultaneously from 4 mm to 10 mm. As can be seen from Fig 3.9 (a), the maximum reflection losses of three cases of slot widths (W_1 = W_2 = 0.6 mm, 1.4 mm, and 3.5 mm) are in the range of -1.3 – -1.5 dB. The reflection phase is then studied in Figure 3.9 (b). Although the phase ranges remain almost unchanged for all of the three cases, the curve gradient becomes slower with increasing slot widths, which is much desired to make the elements more distinguishable in dimension.

Next, the reflection properties are characterized by varying only one of the slot widths. Again, L_1 and L_2 are changed simultaneously (shown in the x-axis). Figure 3.10 shows the reflection losses and S curves for different horizontal slot widths (W_1 = 0.6, 1.4, and 3.5 mm), where the width of the vertical slot is made constant at (W_2 = 1.4 mm). Again, it is observed that the reflection loss can be kept well below -1.5 dB at all slot lengths. With reference to Figure 3.10 (b), a larger slot width is good for lowering changing rate of the reflection phase.

By keeping the horizontal slot width (W_1 = 1.4 mm) unchanged, with reference to Figure 3.11, the effects of vertical slot width are studied for W_2 = 0.6, 1.4, and 3.5 mm. It is observed from simulation that changing W_2 does not affect the phase range of S curve much.

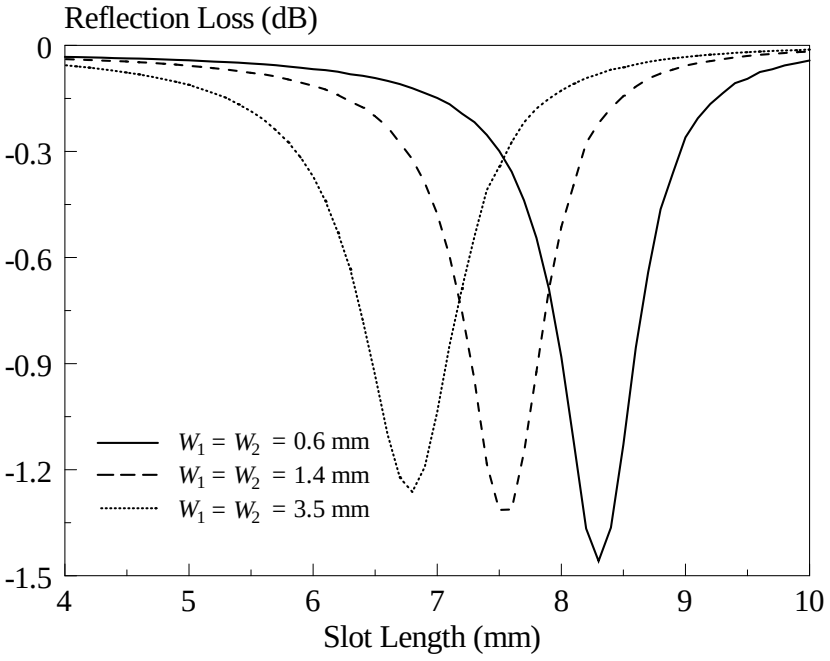

(a)

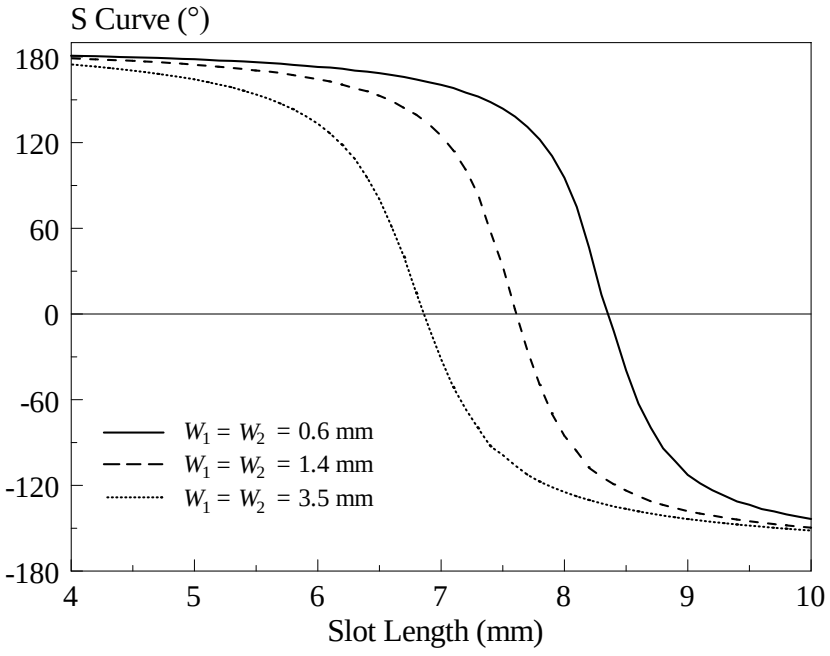

(b)

Figure 3.9: Effects of the Slot Widths (W_1, W_2) on the (a) Reflection Loss; (b) S Curve of the Proposed Cross-Slotted Circular Patch Unit Cell.

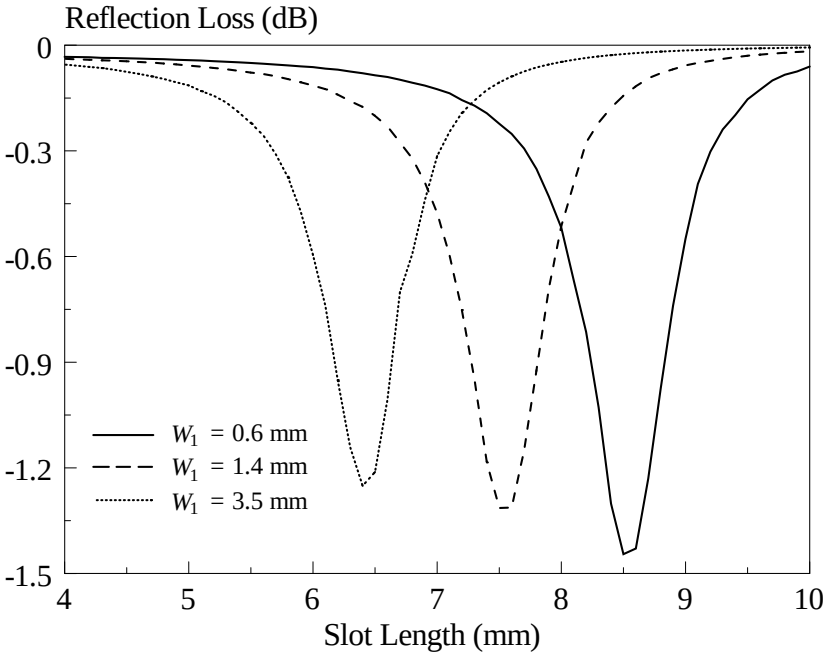

(a)

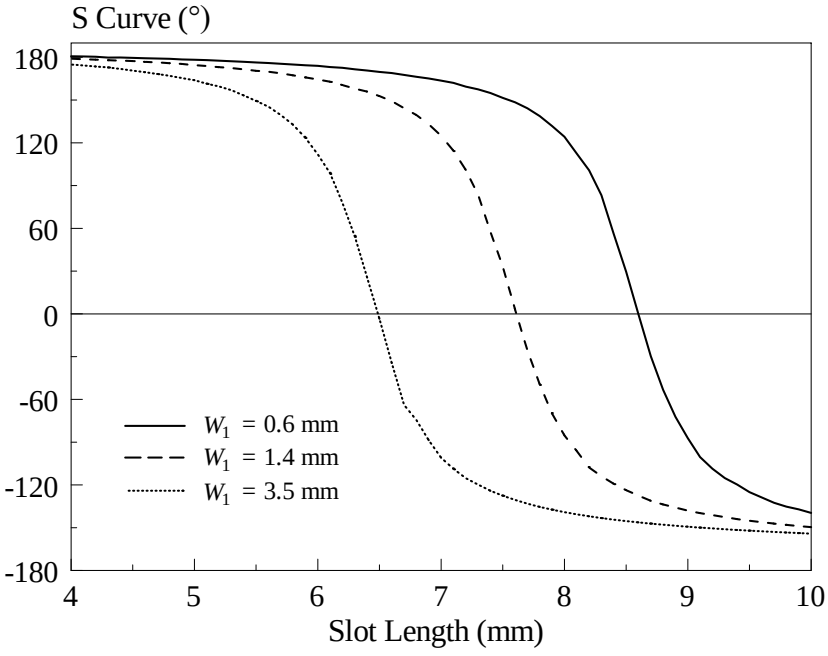

(b)

Figure 3.10: Effects of the Horizontal Slot Width W_1 on the (a) Reflection Loss; (b) S Curve of the Proposed Cross-Slotted Circular Patch reflectarray Unit Cell.

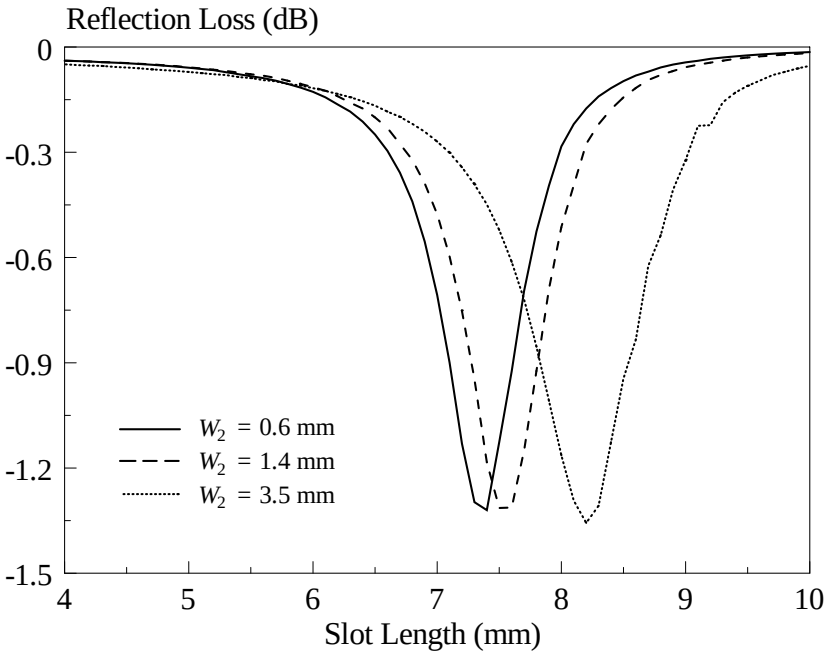

(a)

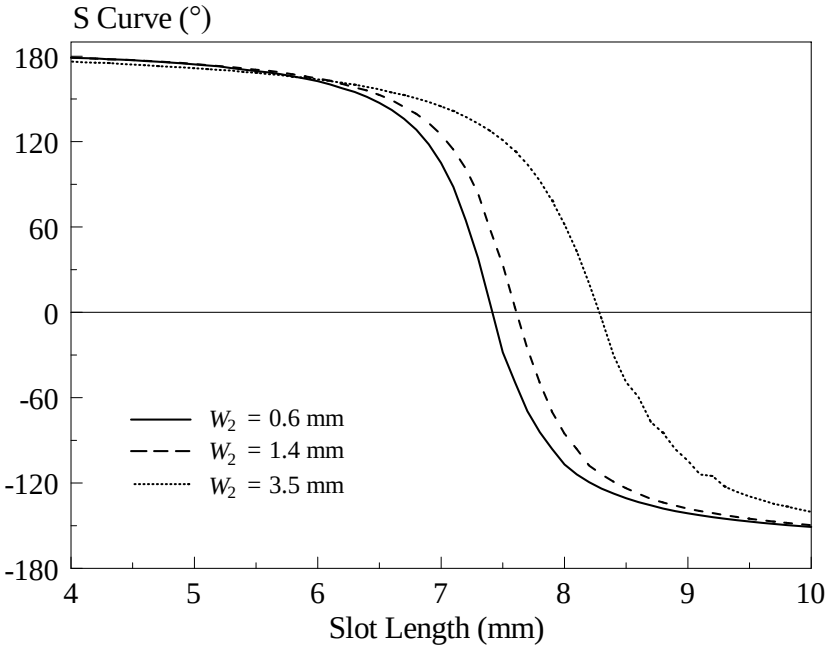

(b)

Figure 3.11: Effects of the Vertical Slot Width W_2 on the (a) Reflection Loss; (b) S Curve of the Proposed Cross-Slotted Circular Patch Reflectarray Unit Cell.

3.5.3 Patch Radius

By keeping the slot widths at $W_1 = W_2 = 1.4$ mm and varying the slot lengths ($L_1 = L_2$) from 2 to 11.5 mm, Figure 3.12 shows the changes in reflection loss and S curve when the patch radius R is varied. It is obvious that making the patch radius smaller is helpful to expand the reflection phase range of the unit element, but at the cost of having a higher reflection loss and a steeper reflection phase slope. Therefore, tradeoff is needed here as designing a reflectarray requires an S curve with broad reflection phase range but slow gradient.

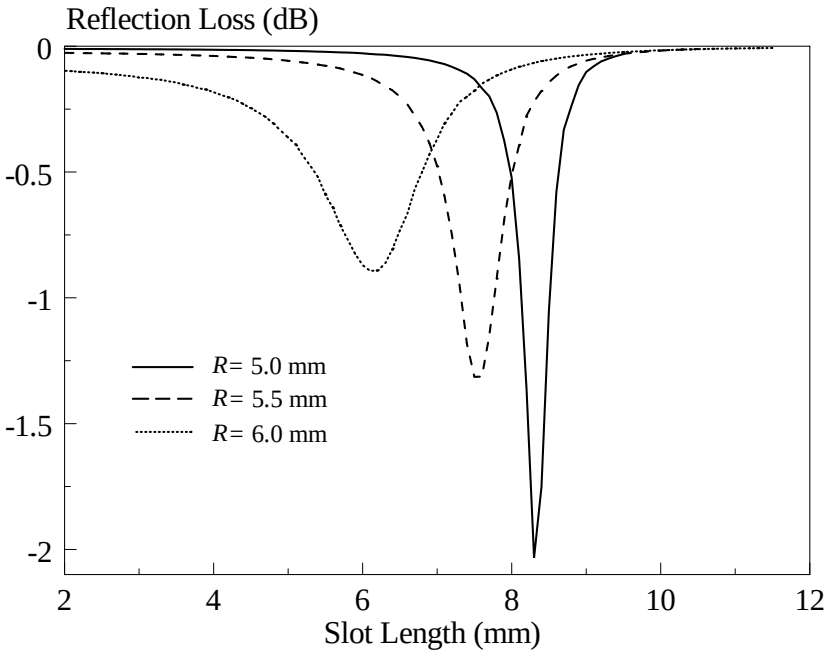

(a)

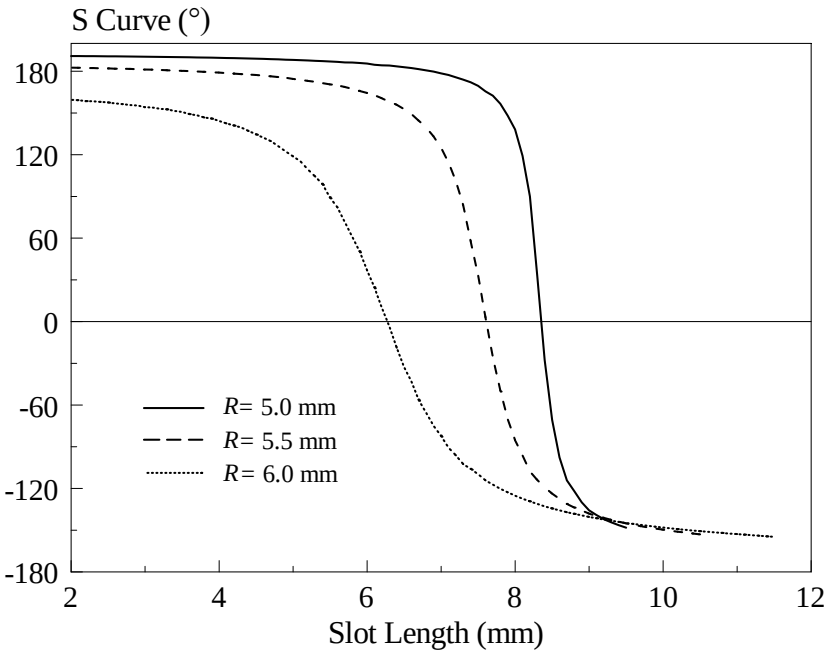

(b)

Figure 3.12: Effects of the Patch Radius *R* on the (a) Reflection Loss; (b) S Curve of the Proposed Cross-Slotted Circular Patch Reflectarray Unit Cell.

3.5.4 Slot Inclination Angle

As can be seen from Figure 3.13, rotating the horizontal (*y*–directed) and vertical (*x*–directed) rectangular slots anticlockwise to any four of the angles (θ = 0°, 22.5°, 45° and 62.5°) simultaneously does not affect the reflection performance of the proposed unit element. For all four cases, the reflection losses are maintained below -1.5 dB and the phase ranges are about 330°.

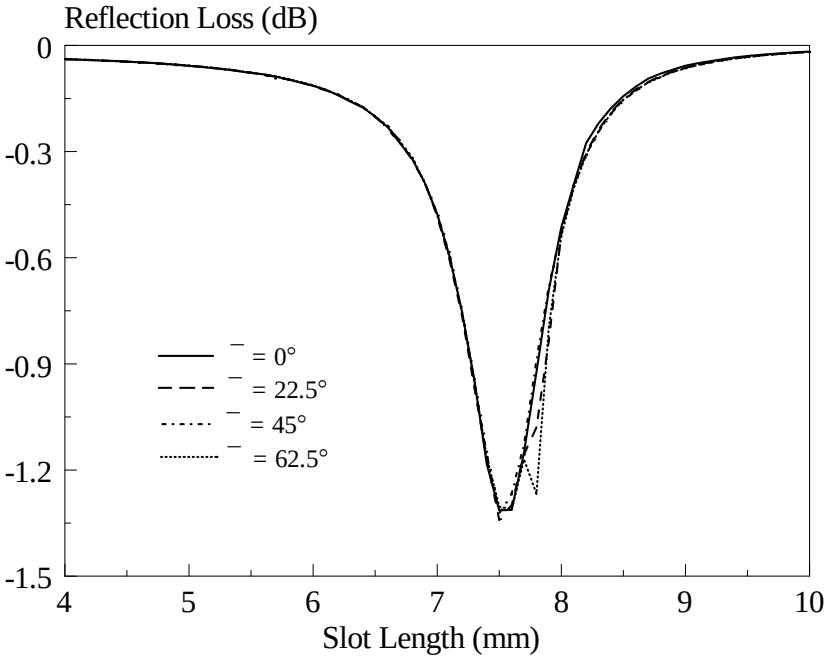

(a)

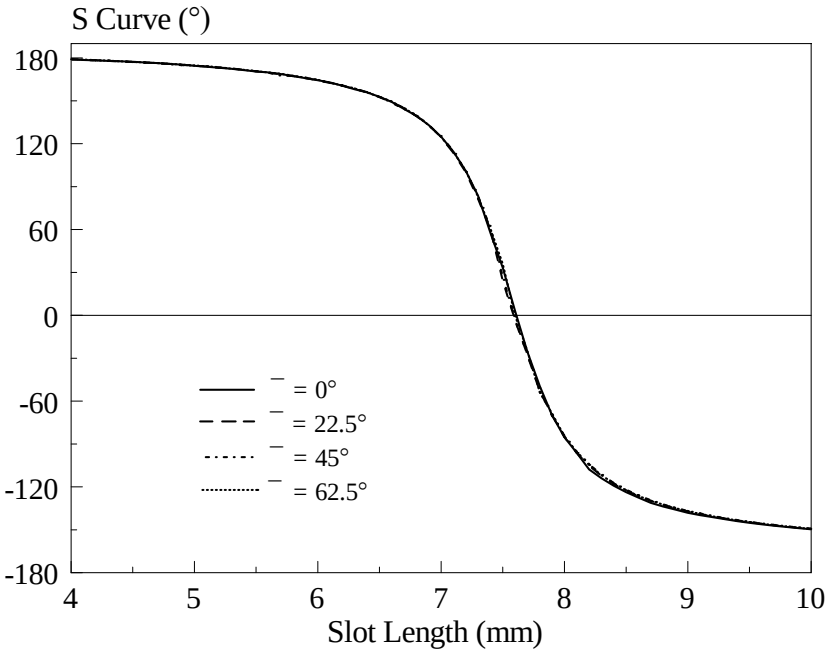

(b)

Figure 3.13: Effects of the Slot Inclination Angle θ on the (a) Reflection Loss; (b) S Curve of the Proposed Cross-Slotted Circular Patch Reflectarray Unit Cell.

3.5.5 Substrate Thickness, Dielectric Constant and Loss Tangent

Substrate with different thicknesses, dielectric constants and loss tangents are simulated. The effect of the substrate thickness (h) is first studied. Referring to Figure 3.14 (a), the reflection loss becomes lower with increasing substrate thickness (h). Referring to Figure 3.14 (b), a thinner substrate is able to provide a larger reflection phase range but with a much steeper S curve. Next, the substrate dielectric constant (ε_r) is studied in Figure 3.15. Although increasing the value of substrate dielectric constant (ε_r) helps to lower the reflection loss, a smaller reflection phase range is obtainable. The substrate loss tangent (tan δ) is now studied. With reference to Figure 3.16, changing the value of substrate loss tangent (tan δ) will only affect the reflection loss performance. Higher reflection loss is observed when the substrate loss tangent (tan δ) is varied from 0.0027 to 0.3, as can be seen from Figure 3.16 (a).

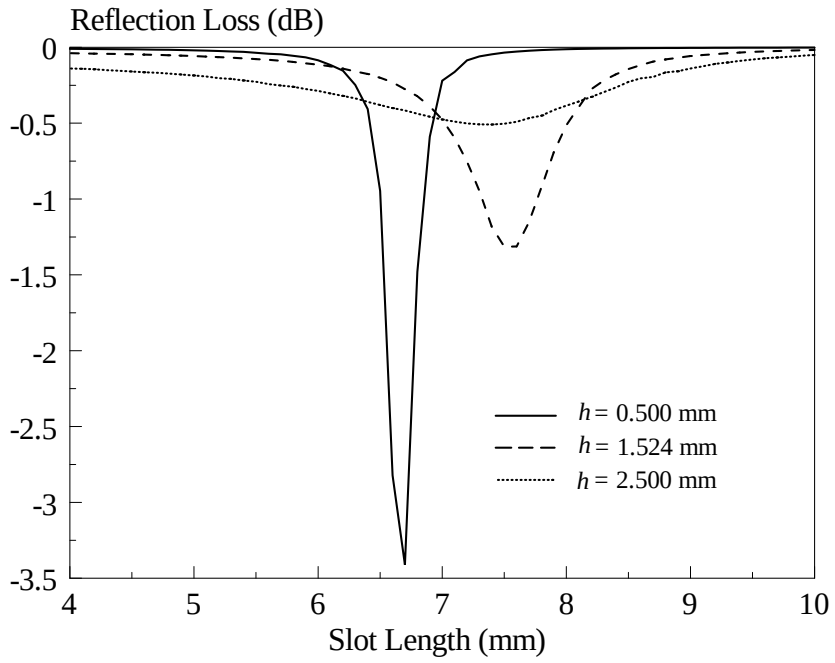

(a)

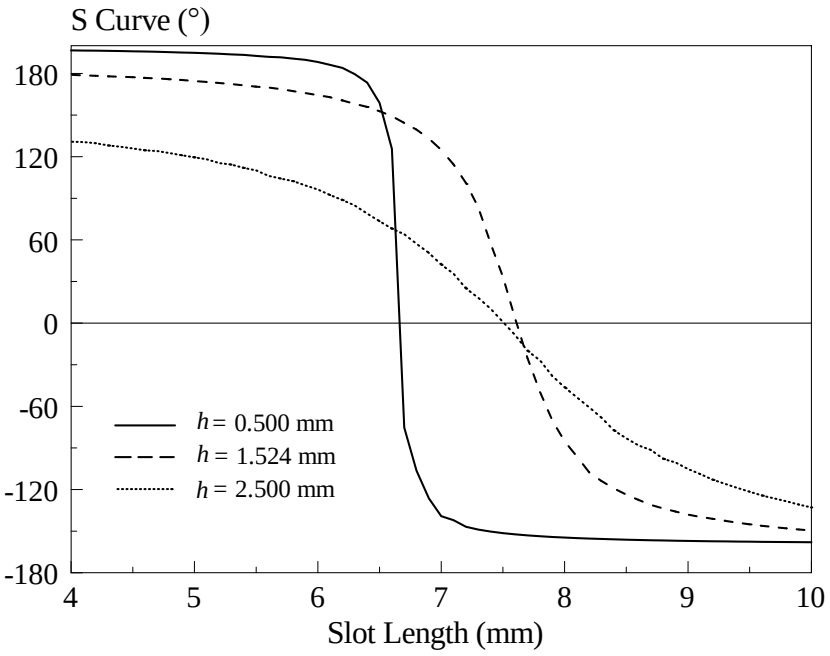

(b)

Figure 3.14: Effects of the Substrate Thickness *h* on the (a) Reflection Loss; (b) S Curve of the Proposed Cross-Slotted Circular Patch Reflectarray Unit Cell.

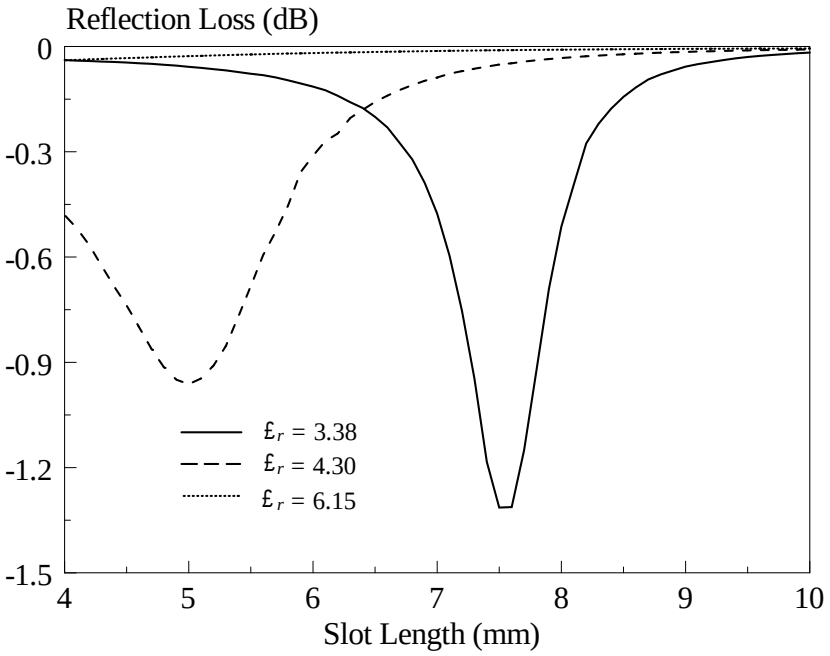

(a)

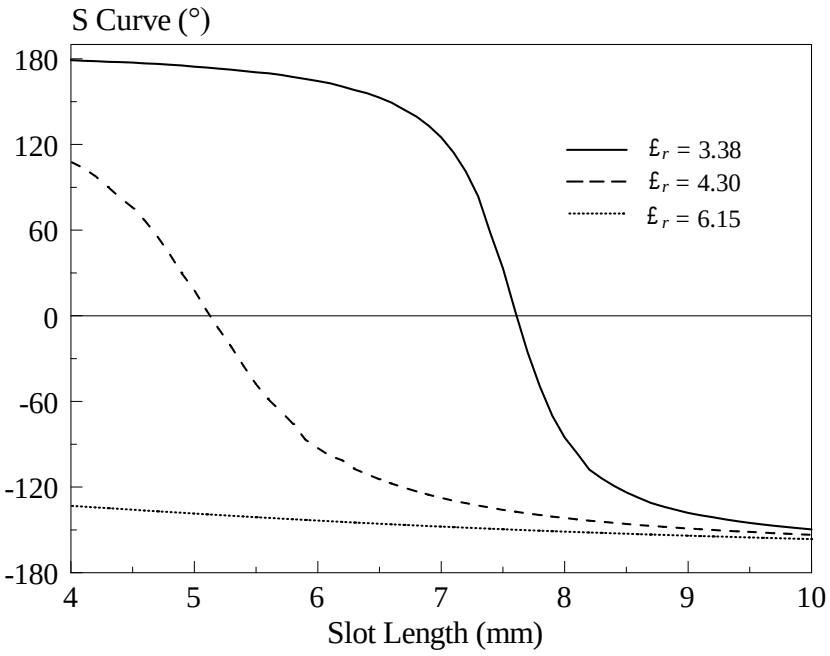

(b)

Figure 3.15: Effects of the Substrate Dielectric Constant ε_r on the (a) Reflection Loss; (b) S Curve of the Proposed Cross-Slotted Circular Patch Reflectarray Unit Cell.

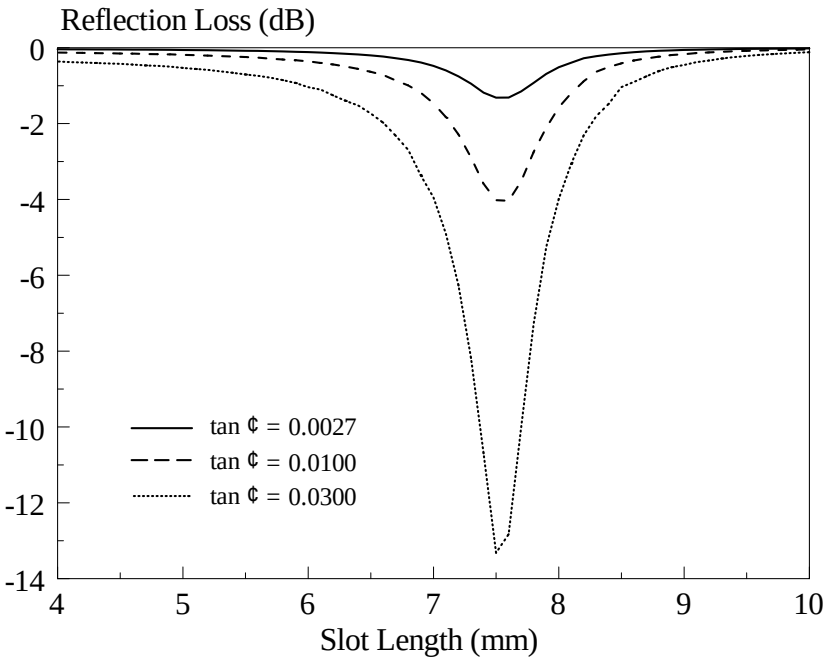

(a)

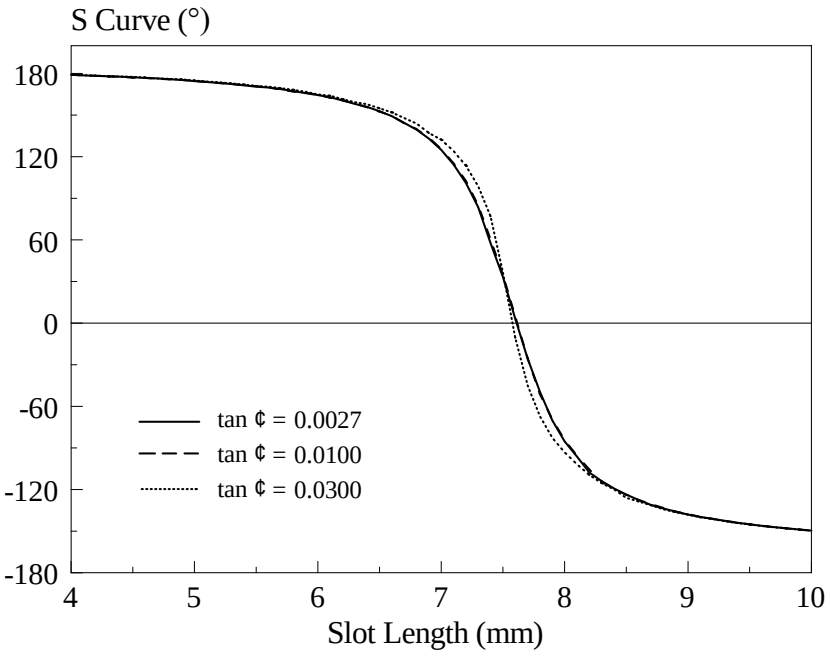

(b)

Figure 3.16: Effects of the Substrate Loss Tangent (tan δ) on the (a) Reflection Loss; (b) S Curve of the Proposed Cross-Slotted Circular Patch Reflectarray Unit Cell.

3.5.6 Comparison of Cross-Slotted Circular and Square Patches

To further study the effects of patch geometry on the reflection characteristics, a square patch (5.5 mm×5.5 mm), which is etched with a cross slot ($L_1 = L_2$ = 10 mm and $W_1 = W_2$ = 1.4 mm), is simulated. The square patch is made to have close footprint as its circular counterpart. In this case, the cross slot is placed at the patch centre (shown in the inset of Figure 3.17 (a)). The reflection loss and S curve of the cross-slotted rectangular patch are presented in Figure 3.17, along with the results of the circular one for ease of comparison. With reference to Figure 3.17 (a), the reflection losses of the patches maximize at different slot lengths, mainly due to their difference in resonance frequencies. Interestingly, it is noted that the reflection phase range of the cross-slotted square patch (~ 230º) is much smaller than its circular counterpart (328.68º) in this case.

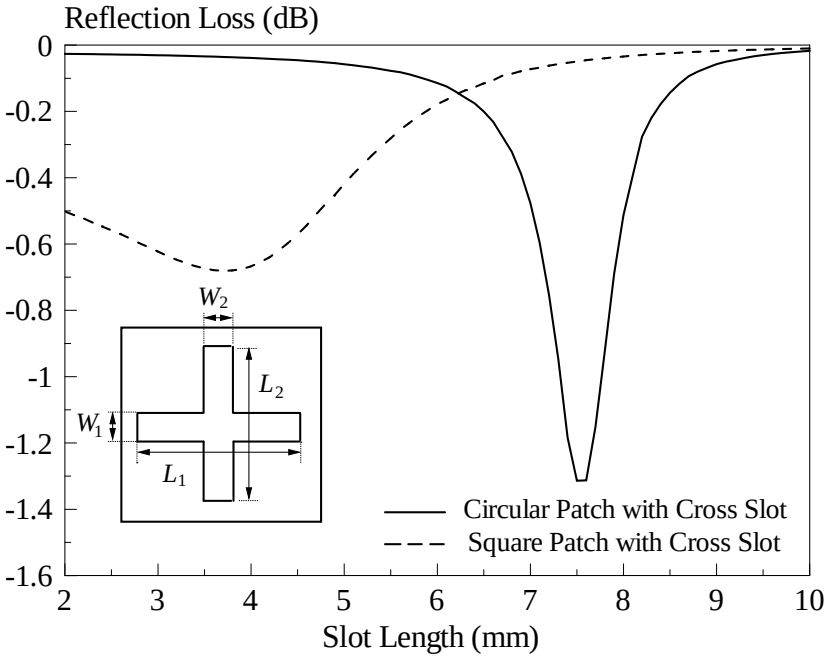

(a)

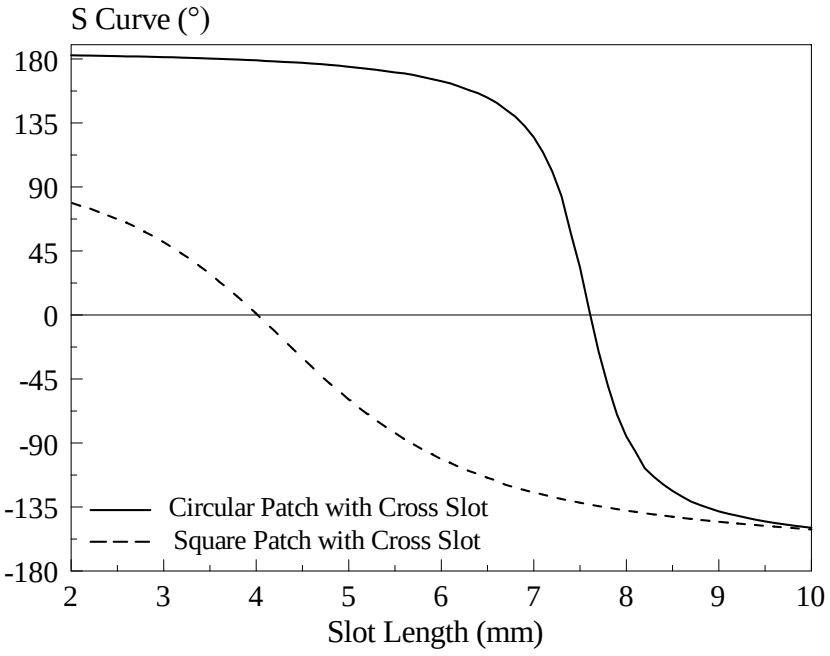

(b)

Figure 3.17: Comparison of the (a) Reflection Losses, (b) S Curves of the Cross-Slotted Circular Patch (R = 5.5 mm) and the Cross-Slotted Square Patch (5.5 mm×5.5 mm) with the Same Slot Dimension ($L_1 = L_2$ = 10 mm and $W_1 = W_2$ = 1.4 mm).

3.6 Conclusion

A cross-slotted circular microstrip patch is explored for reflectarray design. The cross slot is etched centrally and symmetrically at the centre of a circular microstrip patch, the effects of the slot dimensions are investigated. A reflection phase range of 328.68° is achievable. It has been found that the changing rate of the reflection phase can be easily tuned by varying the slot width. In general, large width is good for a slow-changing S curve. It has been demonstrated that using substrate with different thicknesses and dielectric constants are another two possible methods to tune the reflection performance. It has also been shown that, with the same footprint, the cross-slotted circular patch can be made to have a broader phase range than its square counterpart. Good agreement has been found between the simulated and experimental data.

CHAPTER 4

DOUBLE-LAYERED CIRCULAR MICROSTRIP REFLECTARRAY ELEMENT WITH BROAD PHASE RANGE

4.1 Introduction

Parabolic disc and phased array are among the most popular antennas used by various wireless applications. However, the curvature surface of the parabolic antenna has made the manufacturing process difficult and the hardware itself very bulky. For a phased array, many power dividers are usually needed to provide phase shifts, which can be lossy in the high frequency ranges (Huang and Encinar, 2007). In 1963, Berry et al. came up with the earliest concept of reflectarray which was built by cascading the radiating apertures of multiple truncated waveguides (Berry, Malech and Kennedy, 1963). This structure was bulky, and as a result, Berry's invention had not been popular until the introduction of microstrip reflectarrays by John Huang in 1991. A microstrip reflectarray is a thin flat plate structure which consists of many microstrip resonators printed on a grounded substrate. It has many advantages such as low profile, flat surface, and low manufacturing costs (Huang, 1991; Pozar, Targonski and Syrigos, 1997). When used for designing reflectarray, a microstrip unit element is always required to provide low reflection loss, large reflection phase range, and slow changing rate in the S curve.

Various microstrip-based unit elements have been proposed to obtain large reflection phase range and gradual phase slope. In (Chaharmir et al., 2003), a multilayer unit element with variable slot lengths etched on the ground plane is

capable of providing a phase range of 330°. However, a phase range of less than 360° implies that such a unit element is not sufficient to be used for designing large-size reflectarrays. In (Chaharmir, Shaker, Cuhaci and Ittipiboon, 2006; Li, Bialkowski, Sayidmarie and Shuley, 2010; Chaharmir, Shaker, Gagnon and Lee, 2010), it was shown that using various shapes of double ring elements could provide large reflection phase range exceeding 360° with reasonable reflection phase slope. Nonetheless, the gap between the inner ring and the outer ring of the elements has to be made very narrow, usually less than 0.5 mm, making the fabrication process and alignment very difficult. Exploiting the parasitic elements of a multilayer mushroom structure has also been demonstrated to be a possible way to introduce reflection phase shift to an incoming wave (Maruyama et al., 2010a; b, 2011). However, optimization of the reflection phase is greatly dependant on the parasitic capacitance and inductance which may involve massive calculations. The computational process has made the implementation extremely tedious. Later, in (Maddahali and Forooraghi, 2013), the concept of fractal structures was applied for designing a unit element to mitigate mutual coupling effect between the reflectarray elements. Although reflection phase range of 700° was achievable, careful design was required as the structure was somewhat complex.

In this chapter, the microstrip double-layered unit element is explored for reflectarray design. A cross-slotted circular microstrip patch is stacked on top of another solid circular patch for attaining a very broad phase range of 681.82° with low reflection loss. The reflection characteristics are studied for different patch sizes, slot dimensions and substrate dielectric constants. CST Microwave Studio was used for all the simulations while R&S®ZVB8 Vector Network Analyzer (VNA) was deployed for experimental verification.

4.2 Unit Cell Structure

Figure 4.1 illustrates the schematic of the proposed microstrip double-layered reflectarray unit element, which is made on a Duroid RO4003C substrate with thickness of h = 1.524 mm and dielectric constant of ε_r = 3.38. The top layer consists of a circular patch with radius R_1 laminated on Substrate 1. It is etched with a pair of rectangular slots with length of $L_1 = L_2$ and width of $W_1 = W_2$ = 1.4 mm. The slots are placed concentrically at the centre of the circular patch to form a cross as depicted in Figure 4.1 (a). The two rectangular slots are designed in such the way that $L_1 = L_2 = 2 \times (R_1 - 0.5)$. With reference to Figure 4.1 (b), the middle layer consists of a circular patch with radius of R_2 and it is sandwiched in between Substrate 1 and 2. A thin copper lamination which acts as the ground is placed on the bottom-most surface of the structure as shown in Figure 4.1 (c). Figure 4.1 (d) shows a photograph of the fabricated prototype. The reflectarray unit element is modelled using waveguide method. A waveguide working in the C-band (5.8 GHz – 8.2 GHz), with dimension $a \times b \times l$ (34.85 mm × 15.8 mm × 154 mm), is used in both the simulation and measurement.

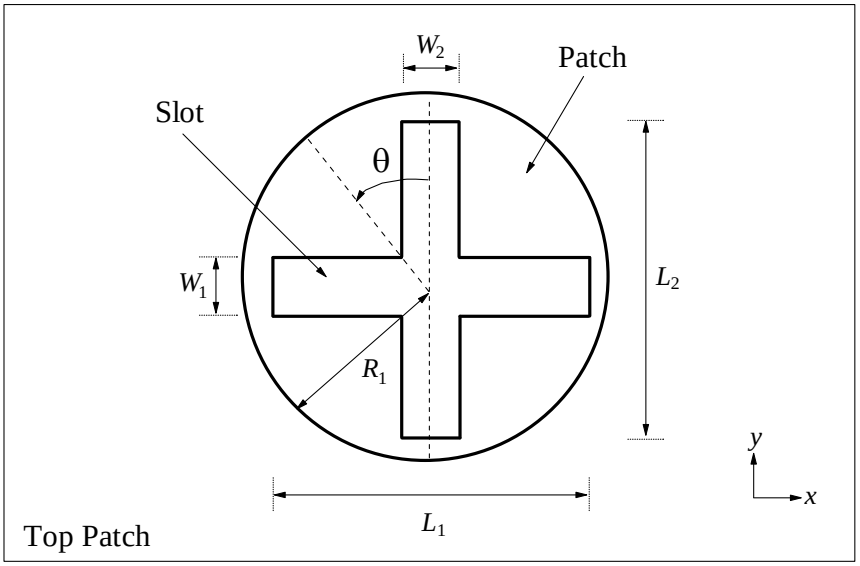

(a)

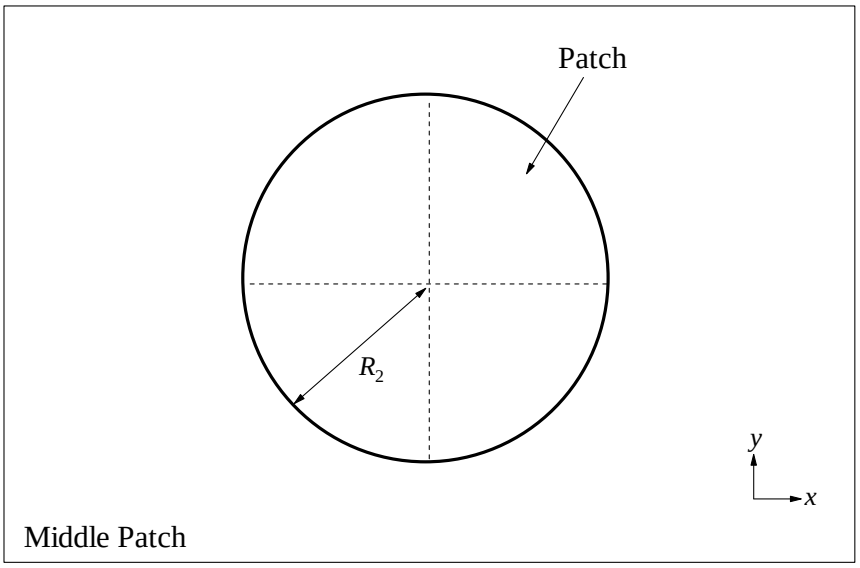

(b)

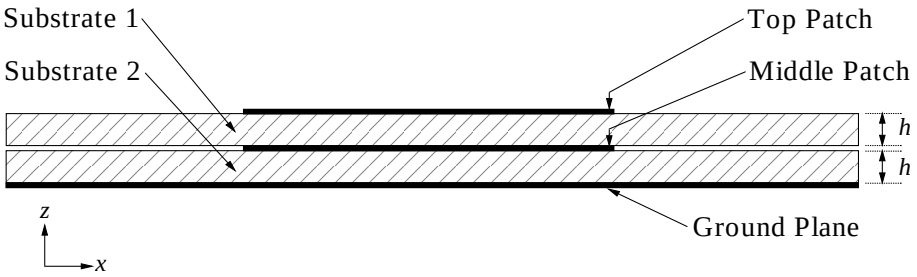

(c)

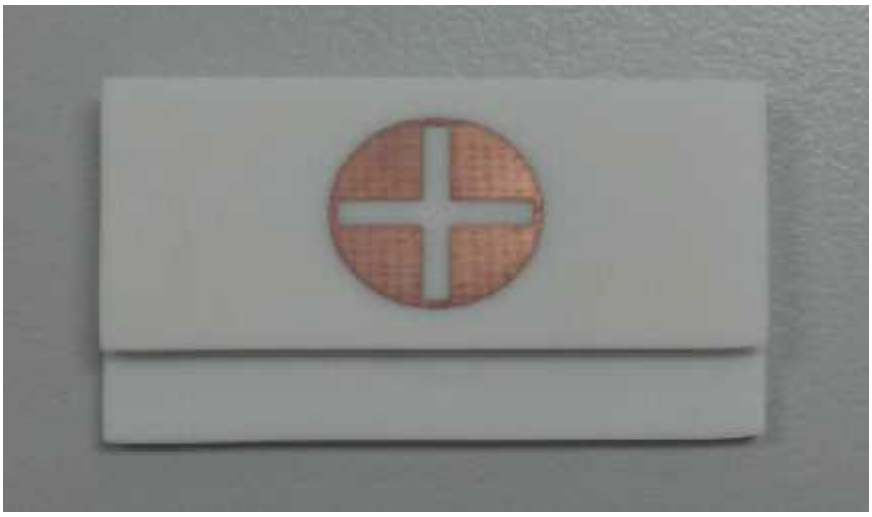

(d)

Figure 4.1: Double-Layered Microstrip Reflectarray Unit Element. (a) Top Patch. (b) Middle Patch. (c) Side View. (d) Photograph of the Fabricated Prototype.

Figure 4.2 (a) depicts the simulation model of the double-layered microstrip reflectarray unit element. With reference to the figure, the reflectarray unit element is placed at one end of the waveguide section and a *y*-polarized wave (6.5 GHz) is generated from another end of the waveguide section, which is also the wave port. The wave propagates towards the direction of the unit element. All of the waveguide boundaries are defined as perfect conductors (PEC). Figure 4.2 (b) illustrates the measurement setup for the waveguide method. With reference to the figure, a coaxial-to-waveguide adaptor is used to connect the waveguide section to the output port of the vector network analyzer (VNA). With the use of a flat shorting plate, de-embedding is conducted so that the reference plane is moved flush to the adaptor flange, making it tally with the simulation setup. The sample is carefully trimmed to make it fit into a rectangular trench with depth of ~ 3mm. With reference to Figure 4.2 (b), the metal plate containing the reflectarray unit element is aligned to cover up the waveguide aperture during the measurement process.

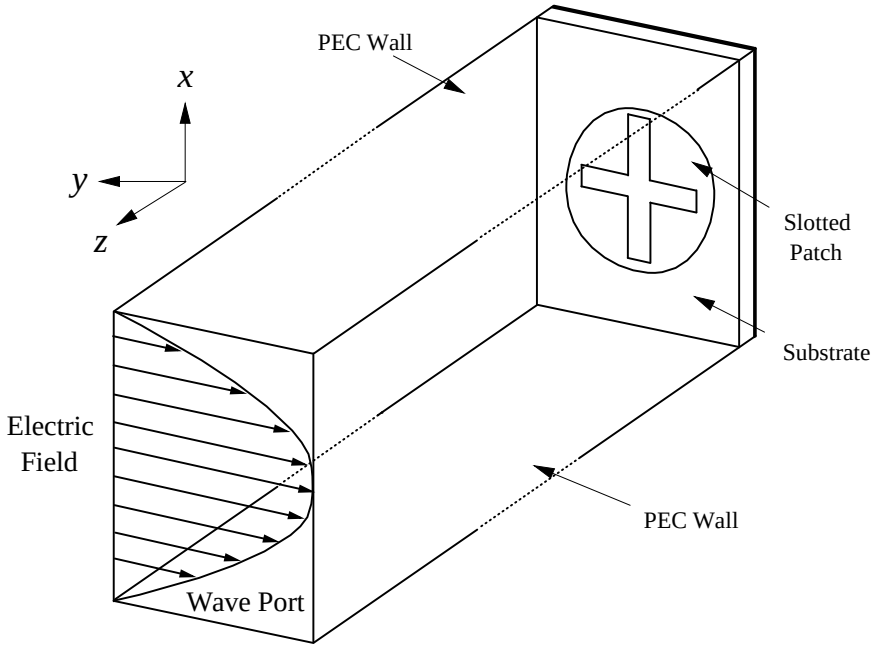

(a)

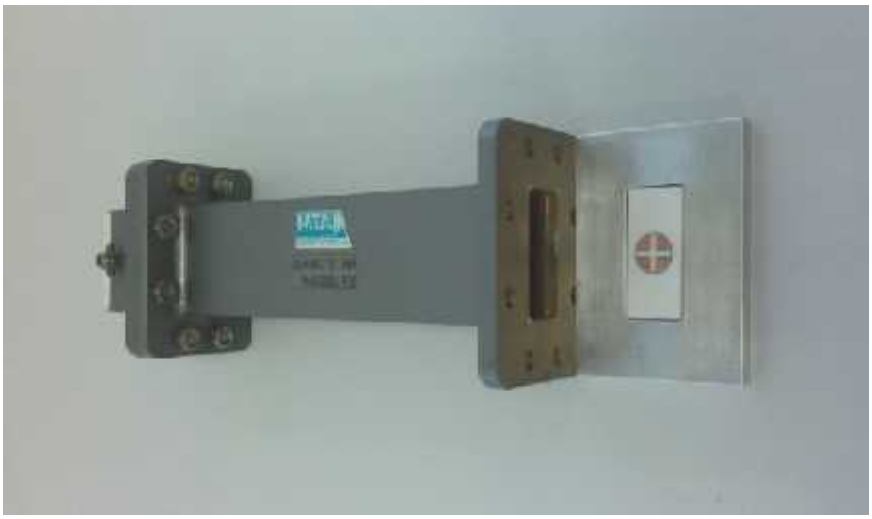

(b)

Figure 4.2: (a) Simulation Model for the Double-Layered Microstrip Reflectarray Unit Element. (b) Experimental Setup for the Waveguide Method.

4.3 Electric Field Distributions

To further understand the patch resonances that enable such a broad phase range, the electric field distributions between the top and middle patches as well as that formed between middle patch and ground are studied for the cases $R_1 = R_2 = 4.7$ mm and 5.7 mm, shown in Figure 4.3 and 4.4 respectively. Comparing Figure 4.3 (a) and 4.4 (a), it is obvious that the two resonances are TM^{z}_{110} mode of the circular microstrip patch resonator (Watkins, 1969; Khor, Lim and Chung, 2014). It simply means that this resonance is excitable in the double-layered structure at these two radii.

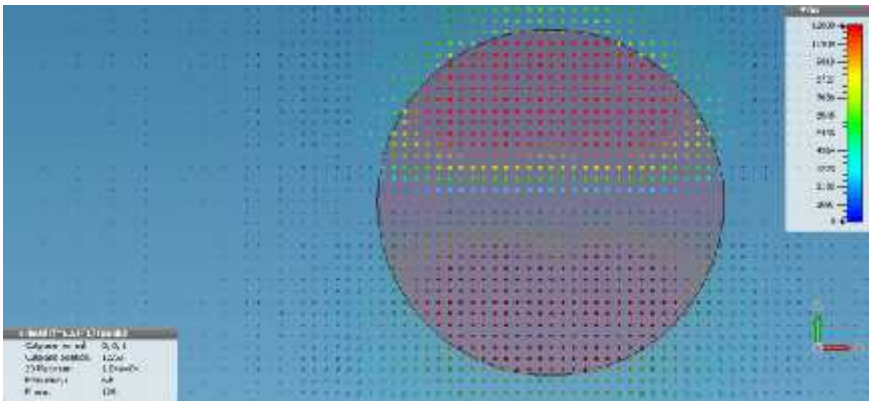

(a)

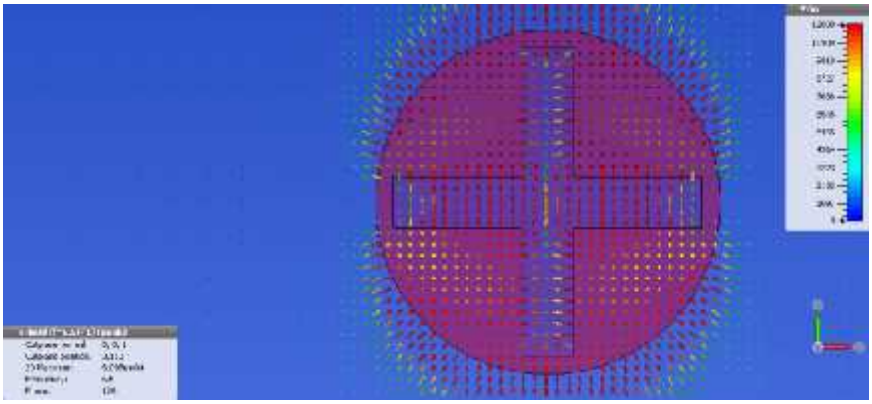

(b)

Figure 4.3: Electric Field Distributions between (a) Middle Patch and Ground at $R_1 = R_2 = 4.7$ mm, (b) Top and Middle Patch at $R_1 = R_2 = 4.7$ mm.

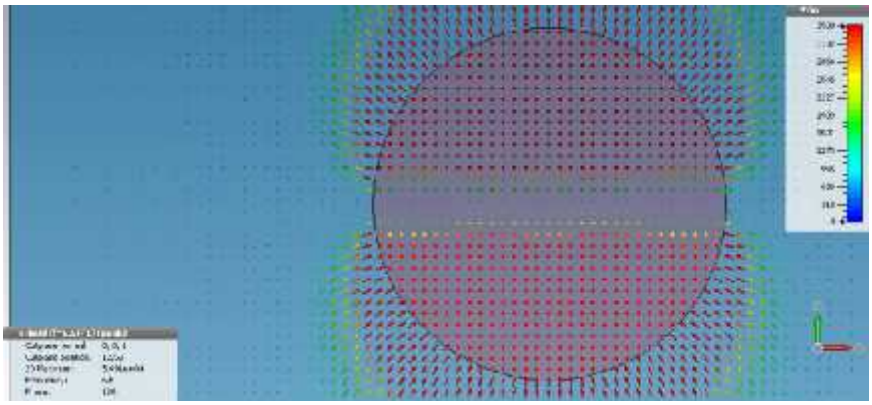

(a)

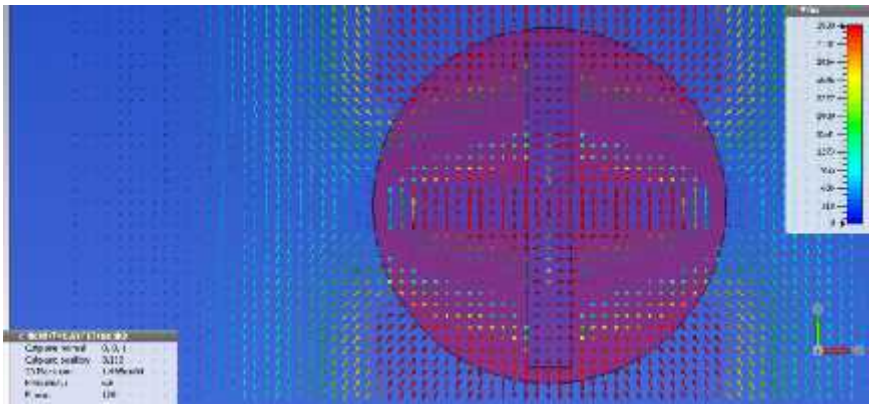

(b)

Figure 4.4: Electric Field Distributions between Middle Patch and Ground at R_1 = R_2 = 5.7 mm, (d) Top and Middle Patch at R_1 = R_2 = 5.7 mm.

4.4 Unit Cell Simulation and Measurement Results

Figure 4.5 depicts the measured and simulated reflection losses and reflection phases (also known as S curves) at the wave port when the patch radius R_2 (= R_1) is varied from 1.5 to 7.5 mm. It can be seen that the measured and simulated reflection losses and reflection phases agree fairly well. Referring to Figure 4.5 (a), two dips are spotted at R_2 = 4.7 mm and R_2 = 5.7 mm with reflection loss not larger than -0.9 dB in measurement. This shows that the proposed unit element has very low loss at all patch dimensions, which is helpful for increasing radiation efficiency of the reflectarray. Figure 4.5 (b) shows the measured and simulated reflection phases. With reference to the figure, a gradual decreasing phase slope with a total reflection phase range of 681.82° has successfully been achieved. Having a large phase range exceeding 360° implies that the proposed unit element can be used to design large-size reflectarrays.

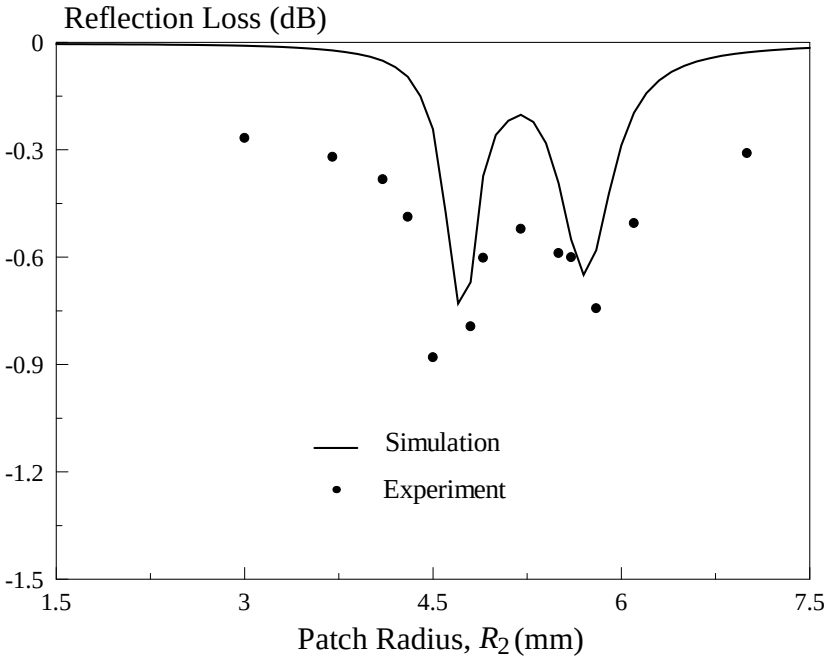

(a)

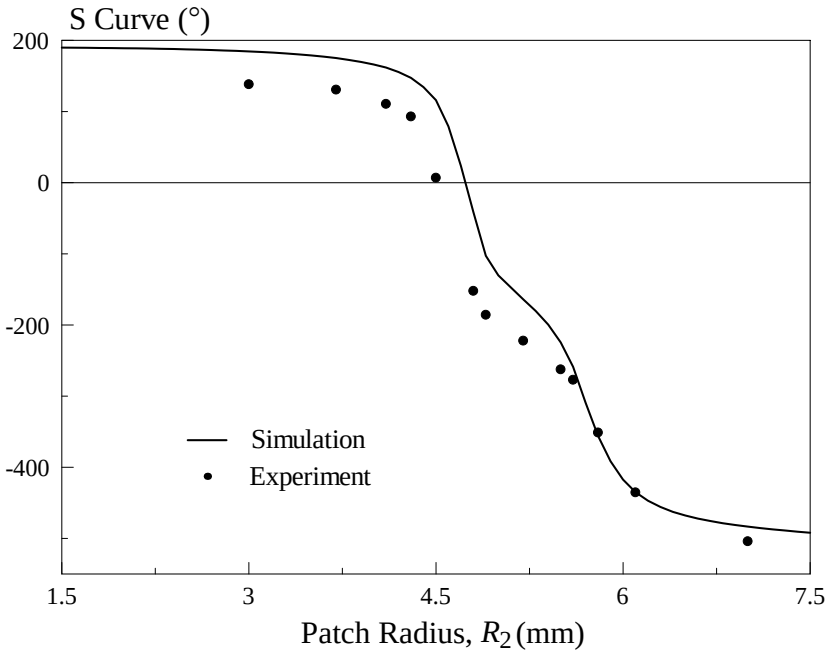

(b)

Figure 4.5: Measured and Simulated (a) Reflection Losses; (b) S Curves of the Proposed Double-Layered Reflectarray Unit Element.

The frequency response is now studied. Figure 4.6 shows the measured and simulated reflection losses and reflection angles of the proposed unit element for the dimension of R_1 = R_2 = 6.1 mm. Good agreement has been found between the measured and simulated results. With reference to Fig 4.6 (a), it is obvious that the measured and simulated curves are in the same trend, with slight discrepancy. The additional ~ 0.5dB loss in measurement can be introduced by the SMA connector (shown in Figure 4.2 (b)), which is not accounted for in simulation. With reference to Figure 4.6 (b), the discrepancy between the measured and simulated reflection phase is not larger than 0.5%, which is acceptable.

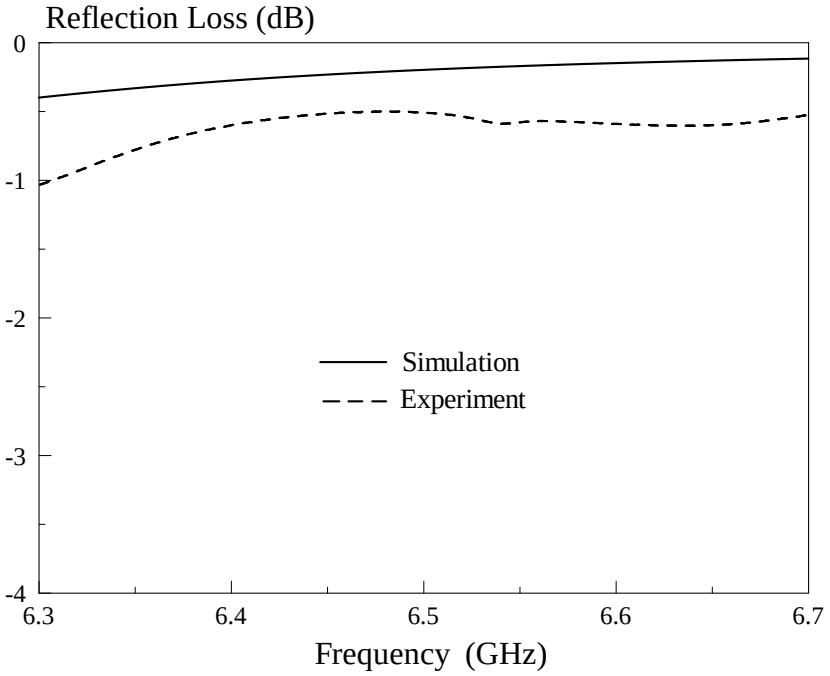

(a)

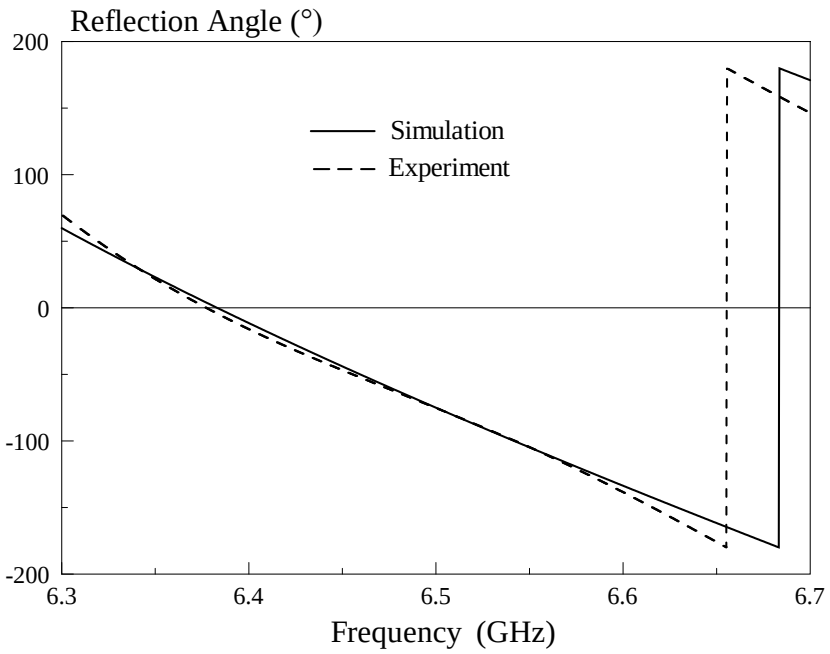

(b)

Figure 4.6: Measured and Simulated (a) Reflection Losses; (b) Angles of Reflection against Frequency for $R_1 = R_2 = 6.1$ mm of the Proposed Double-Layered Reflectarray Unit Element.

4.5 Parametric Analysis

In this section, a complete parametric analysis has been conducted on the important design parameters such as slot length and slot width, slot inclination angle, and patch radius to study the reflection characteristics of the proposed microstrip double-layered unit element. The effects of the substrate thickness, dielectric constant, and loss tangent are also studied. Finally, unit elements with different combinations of top and middle circular patches are explored.

4.5.1 Slot Length

The effect of the horizontal slot length (L_1) is studied first. With reference to Figure 4.7, the patch radii ($R_1 = R_2$) are varied simultaneously from 1.5 to 7.5 mm and the vertical slot length (L_2) is varied as a function of the top patch radius ($L_2 = 2 \times (R_1 – 0.5)$). Referring to Figure 4.7 (a), it is observed that longer slot introduce higher loss. Referring to Figure 4.7 (b), varying the slot length (L_1) will only affect the gradient of the S curve when the patch radius (R_2) is more than 6 mm. Also observed is that the phase change becomes faster with increasing reflection loss.

The effect of the vertical slot length (L_2) is studied next. The patch radii ($R_1 = R_2$) are again varied at the same time from 1.5 to 7.5 mm, but this time, the horizontal slot length (L_1) is varied as a function of the top patch radius ($L_1 = 2 \times (R_1 – 0.5)$). As can be seen from Figure 4.8, changing the slot length (L_2) does not affect the reflection performance much. For all three cases, the reflection loss and S curve are about the same.

The effect of the slot lengths (L_1, L_2) is now studied. Again, R_1=R_2. With reference to Figure 4.9, varying the lengths of the horizontal (L_1) and vertical (L_2) slots concurrently will have effects on the reflection loss and S curve. The same trend is observed when only the length of the horizontal (L_1) slot is varied. For all three studies, the reflection phase ranges are all more than 650°.

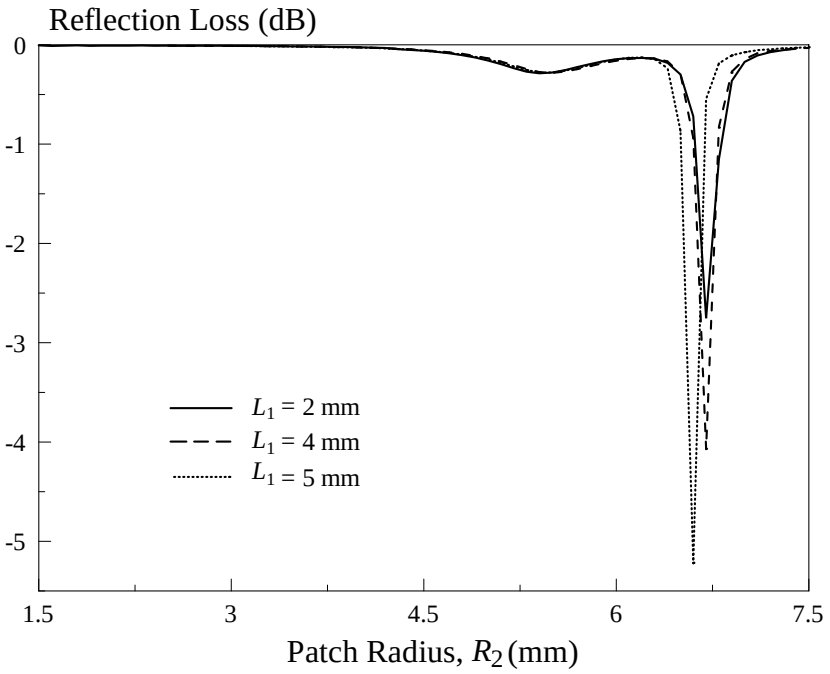

(a)

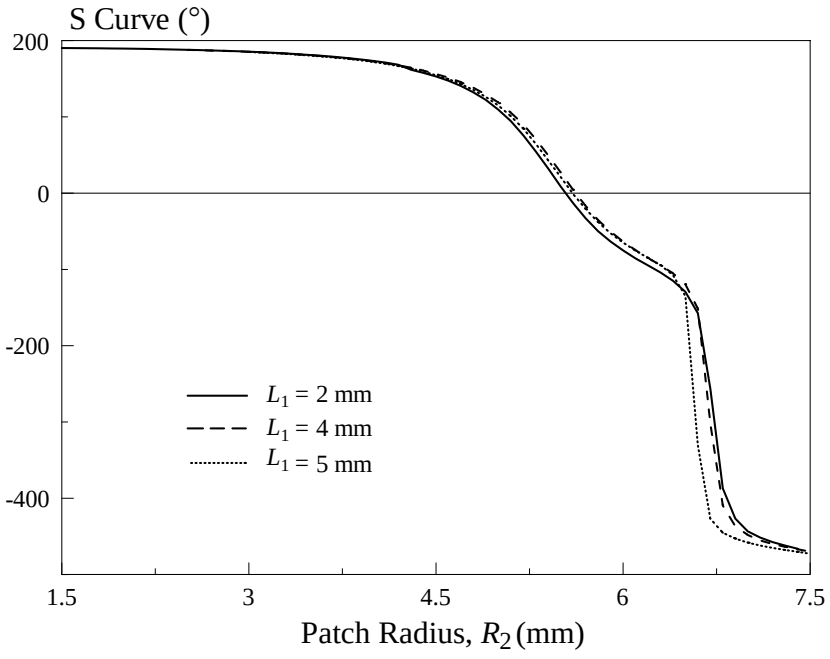

(b)

Figure 4.7: Effects of the Horizontal Slot Length L_1 on the (a) Reflection Loss; (b) S Curve of the Proposed Double-Layered Reflectarray Unit Element.

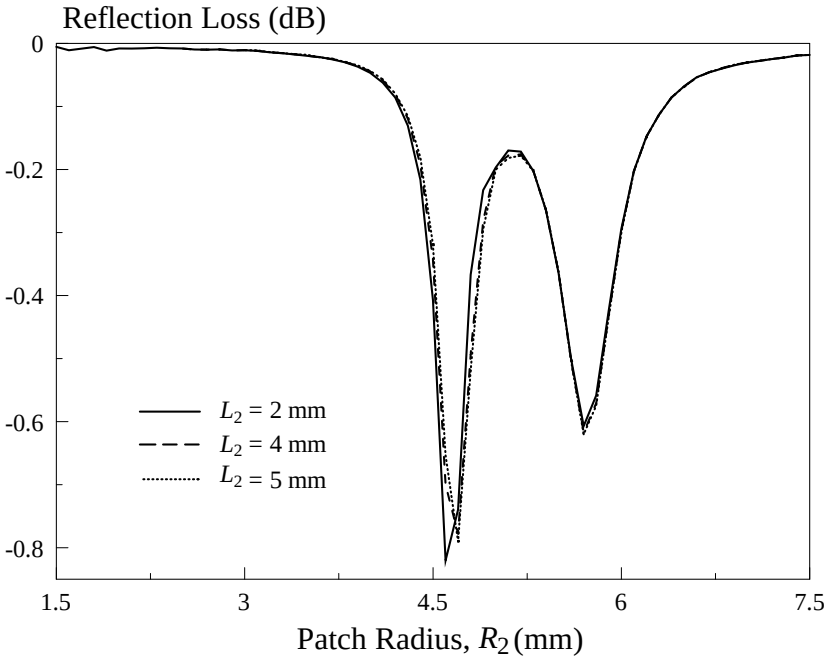

(a)

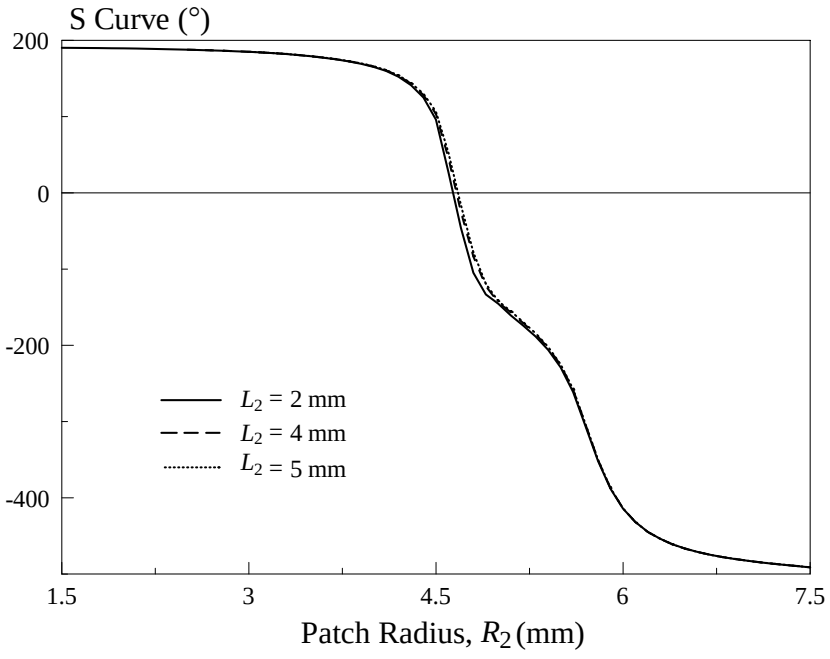

(b)

Figure 4.8: Effects of the Vertical Slot Length L_2 on the (a) Reflection Loss; (b) S Curve of the Proposed Double-Layered Reflectarray Unit Element.

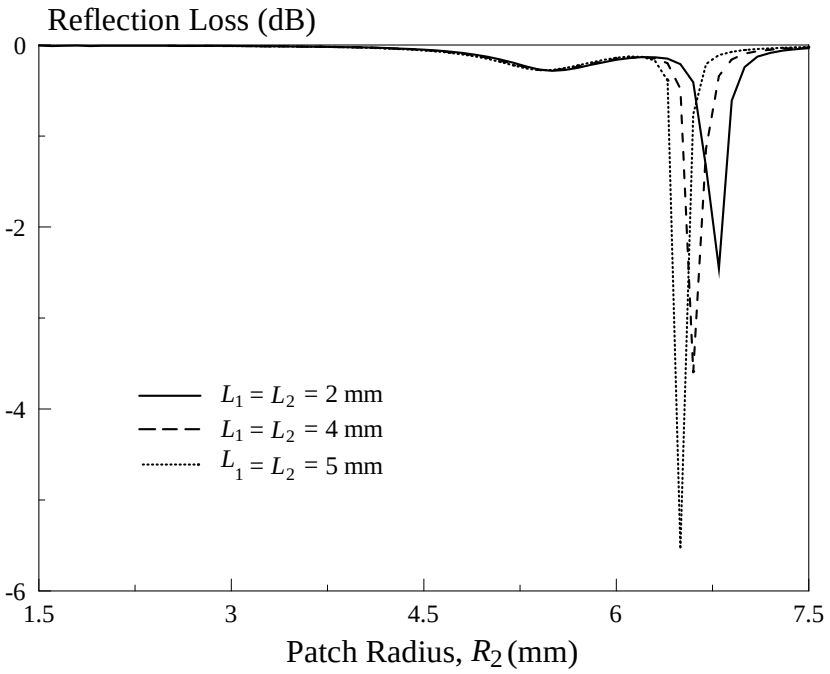

(a)

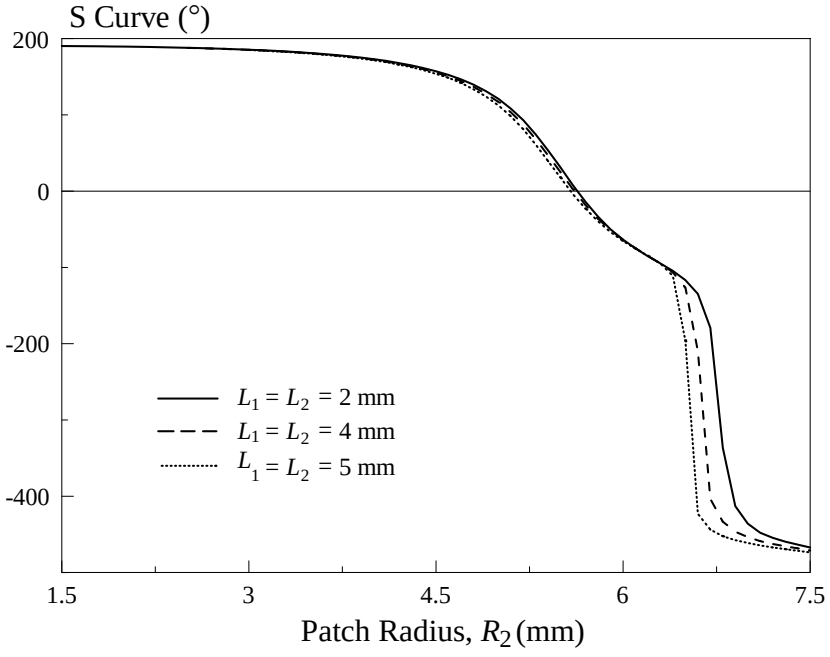

(b)

Figure 4.9: Effects of the Slot Lengths (L_1, L_2) on the (a) Reflection Loss; (b) S Curve of the Proposed Double-Layered Reflectarray Unit Element.

4.5.2 Slot Width

In this section, the effects of changing slot widths, with the patch radii (R_1 = R_2) varied from 1.5 to 7.5 mm, are studied. In the first case, the horizontal slot width (W_1) is varied from 0.3 to 2.5 mm while letting the vertical slot width (W_2) fixed at 1.4 mm. With reference to Figure 4.10 (a), for all three cases, their maximum reflection losses can be kept well below -1.5 dB. With reference to Figure 4.10 (b), the slope change of the reflection phase becomes slower with increasing slot width (W_1), which is much desired as it makes the unit elements more distinguishable in dimension. Similar reflection characteristics are observed when the widths of the horizontal (W_1) and vertical (W_2) slots are changed synchronously, shown in Figure 4.12.

In the second study, the vertical slot width (W_2) is varied while having the horizontal slot width (W_1) set at 1.4 mm. Referring to Figure 4.11 (a), the maximum reflection losses of all three cases (for slot widths of W_2 = 0.3, 1.4 and 2.5 mm) are in the range of 0.5 – 0.9 dB. Referring to Figure 4.11 (b), increasing the slot width (W_2) will in turn increase the changing rate of the S curve. The effect is exactly opposite to that of the case in the first study. It should also be mentioned that varying the slot widths does not degrade the phase range in the two cases.

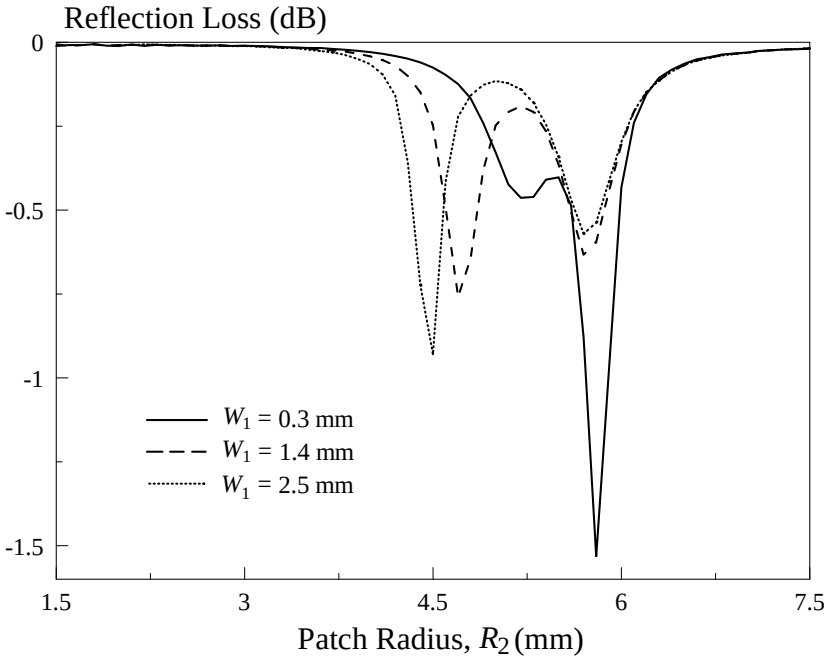

(a)

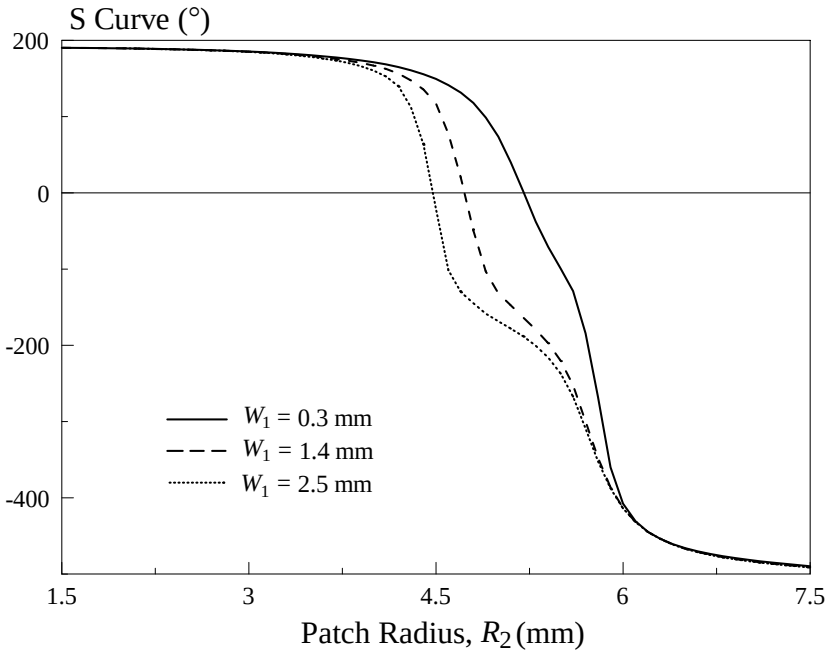

(b)

Figure 4.10: Effects of the Horizontal Slot Width W_1 on the (a) Reflection Loss; (b) S Curve of the Proposed Double-Layered Reflectarray Unit Element.

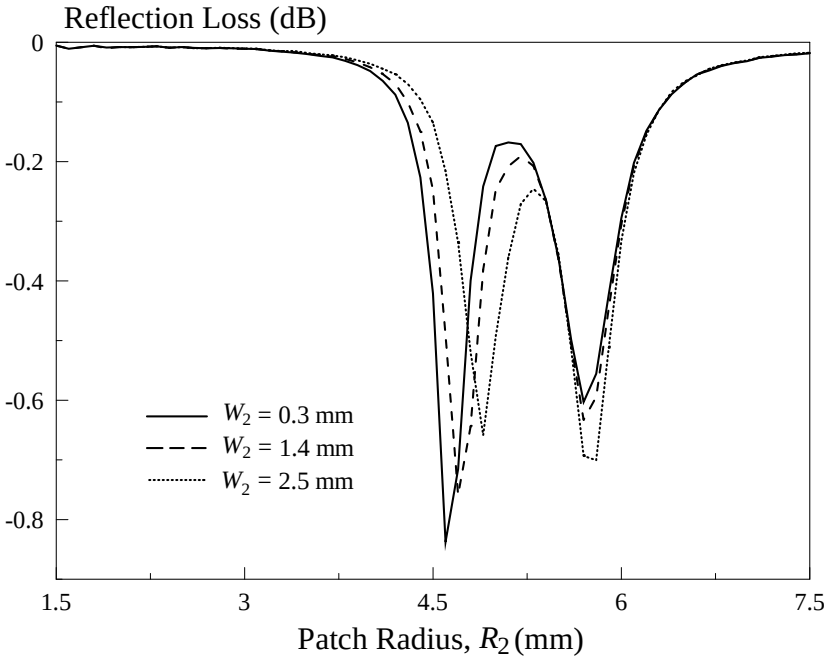

(a)

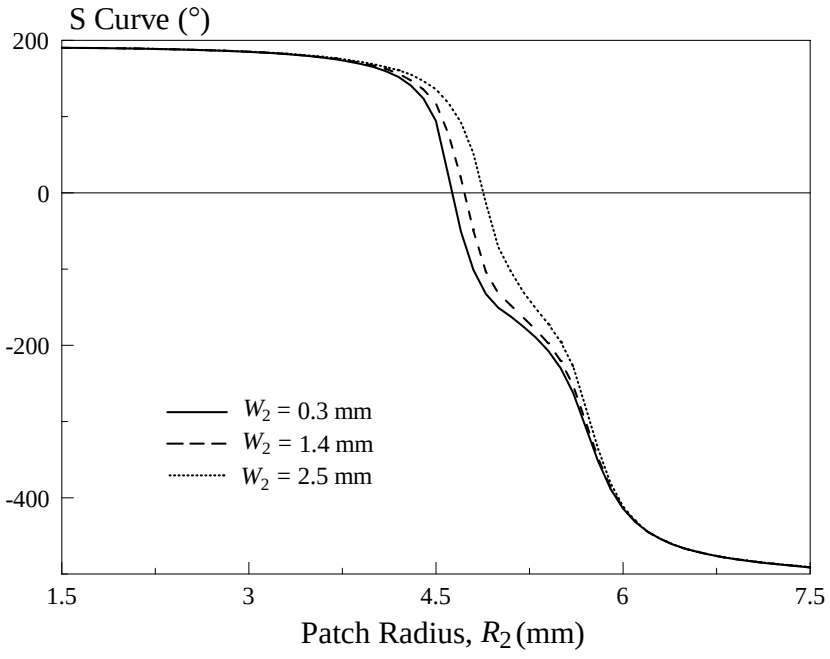

(b)

Figure 4.11: Effects of the Vertical Slot Width W_2 on the (a) Reflection Loss; (b) S Curve of the Proposed Double-Layered Reflectarray Unit Element.

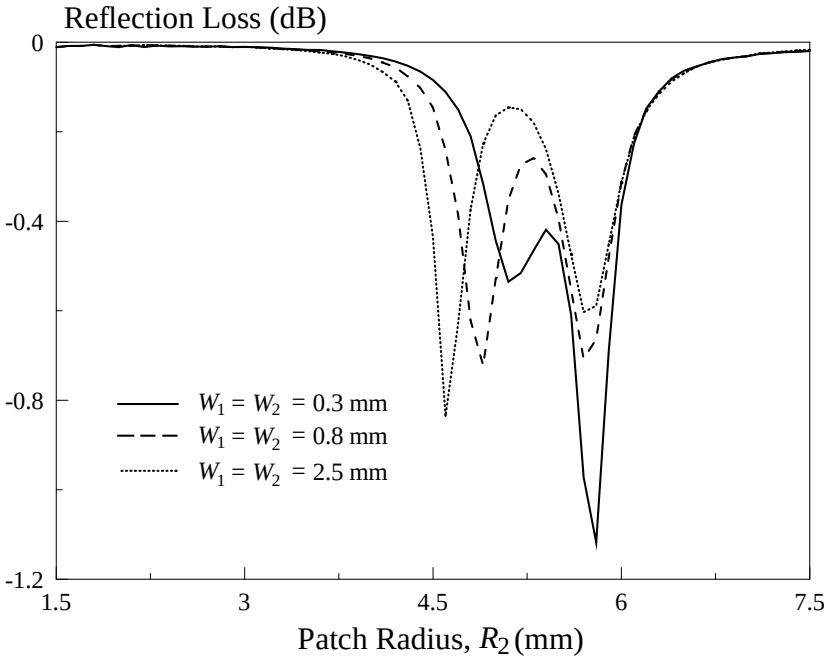

(a)

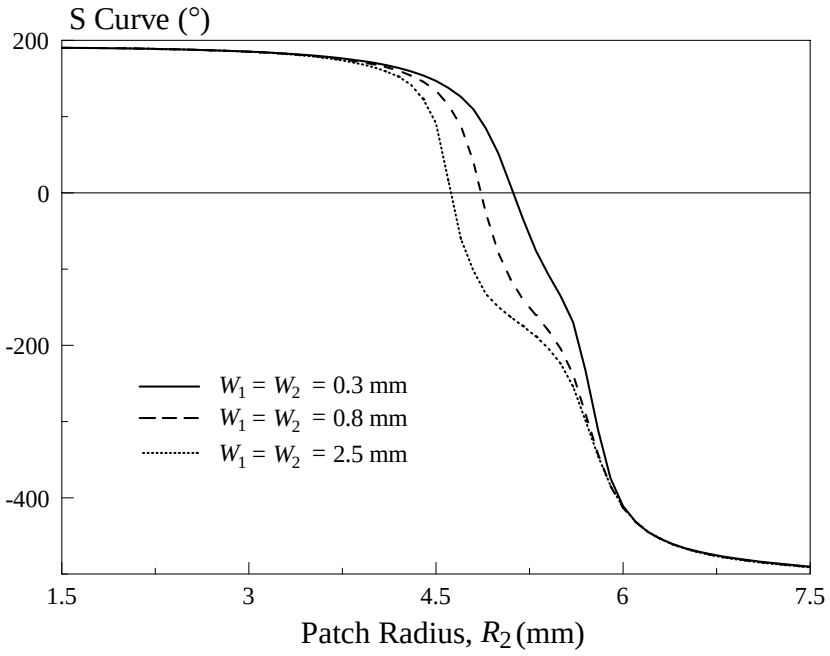

(b)

Figure 4.12: Effects of the Slot Widths (W_1, W_2) on the (a) Reflection Loss; (b) S Curve of the Proposed Double-Layered Reflectarray Unit Element.

4.5.3 Patch Radius

The effects of the radii of the top patch (R_1) and the middle patch (R_2) are studied. In the first study, with reference to Figure 4.13, the radius of the middle circular patch (R_2) is varied from 1 to 7.5 mm while the slot lengths are varied as a function of top patch radius ($L_1 = L_2 = 2 \times (R_1 - 0.5)$). As can be seen from Figure 4.13 (a), the reflection losses for R_1 = 2 mm and R_1 = 7 mm peak at ~ -0.55 dB. Referring to Figure 4.13 (b), steeper reflection phase curve is obtained when the radius of top patch (R_1) is increased from 2 to 7 mm. For both cases (R_1 = 2 and 7 mm), a reflection phase range of not more 360° is achievable.

In the second study, with reference to Figure 4.14, the radius of the top circular patch (R_1) is varied from 1.5 to 7.5 mm and the slot lengths are changed accordingly to the radius of circular patch ($L_1 = L_2 = 2 \times (R_1 - 0.5)$). Regardless of the value of R_2, as can be seen from Figure 4.14 (a), the double-layered structure has its resonant frequency of around 6.5 GHz when R_1 approaches ~ 4.7 mm, which can be justified from the loss performance. Higher loss is induced as the radius of the middle circular patch becomes larger. Steeper phase slope is obtainable by increasing the radius of the middle circular patch from 2 to 7 mm, as can be observed in Figure 4.14 (b). Also referring to the same figure, it is noted that a patch with R_2 = 5 mm has a much greater reflection phase range than other two (R_2 = 2 mm and 7mm).

The effect of radius difference ($d_1 = R_2 - R_1$), where the two patches are varied at the same time and $R_2 > R_1$, is now studied. Figure 4.15 (a) compares the reflection losses for different d_1. Referring to the curves in Figure 4.15 (b), it can be seen that the slope changing rate can be tuned by creating a radius difference in the top and middle patches. For all cases, the phase ranges are greater than 650°. Abrupt gradient change should be avoided.

The effect of radius difference ($d_2 = R_1 - R_2$ where $R_1 > R_2$), where the two patches are varied simultaneously, is then studied. Reflection loss of not larger than -0.8 dB is observed in Figure 4.16 (a). With reference to Figure 4.16 (b), by introducing larger radius difference (d_2) between the two patches, the gradient of the S curve can be made slower at the expense of smaller reflection phase range.

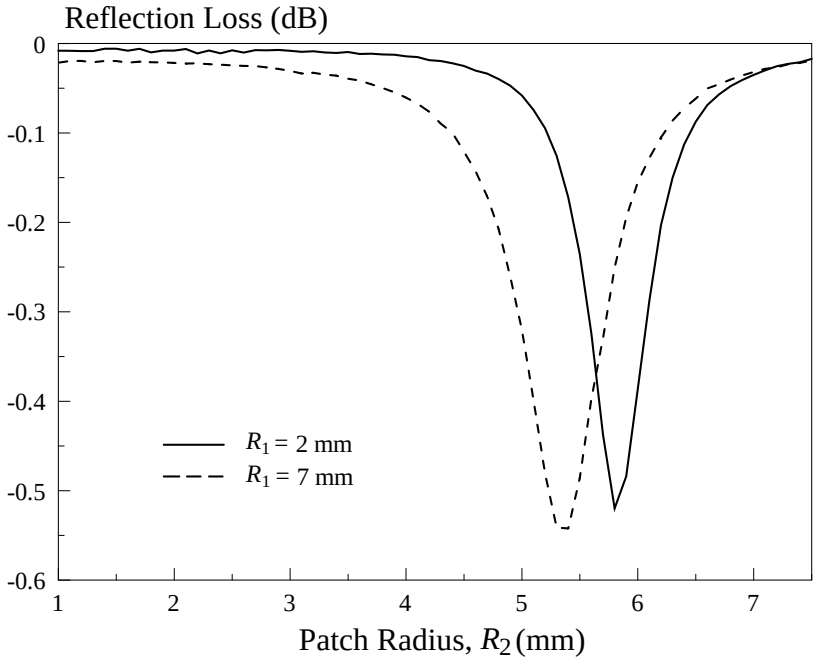

(a)

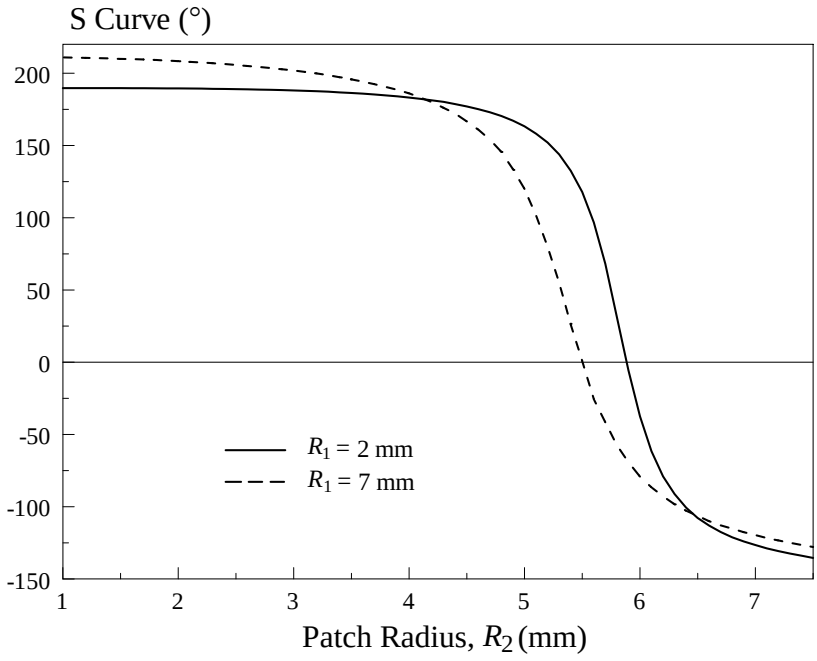

(b)

Figure 4.13: Effects of the Top Circular Patch Radius R_1 on the (a) Reflection Loss; (b) S Curve of the Proposed Double-Layered Reflectarray Unit Element.

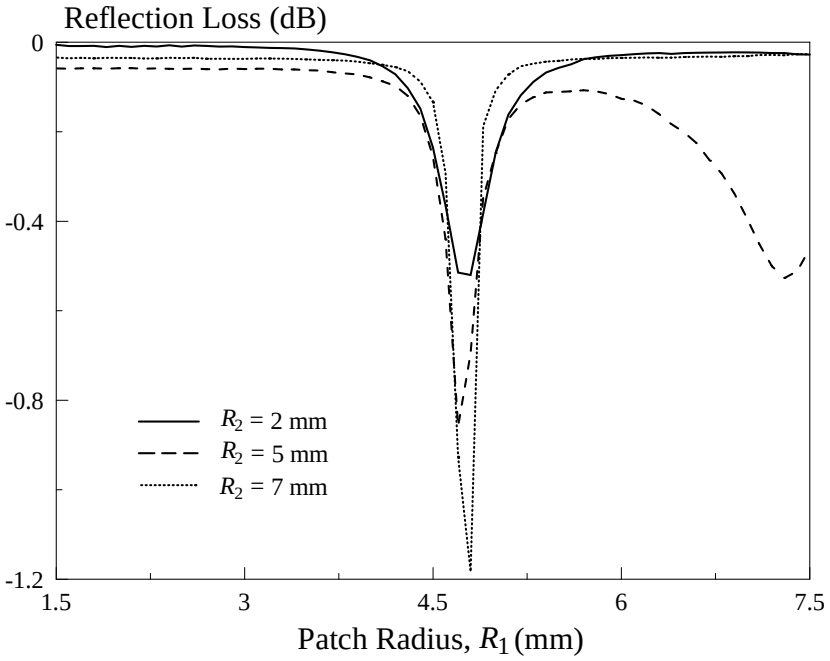

(a)

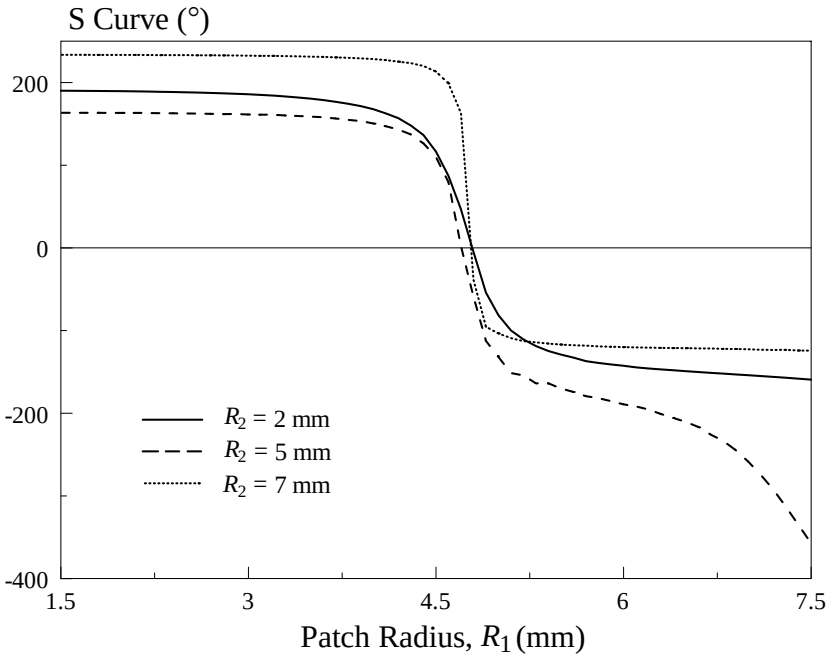

(b)

Figure 4.14: Effects of the Middle Circular Patch Radius R_2 on the (a) Reflection Loss; (b) S Curve of the Proposed Double-Layered Reflectarray Unit Element.

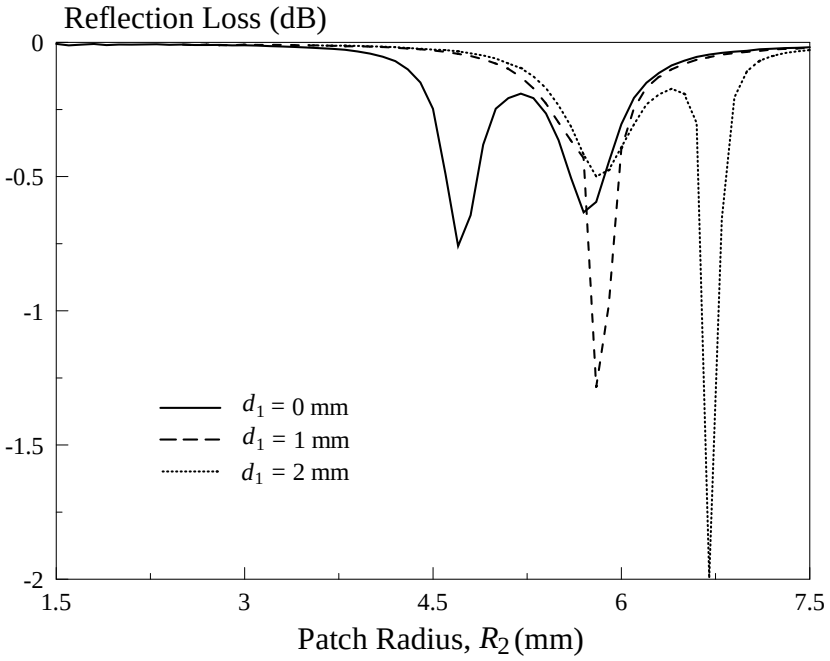

(a)

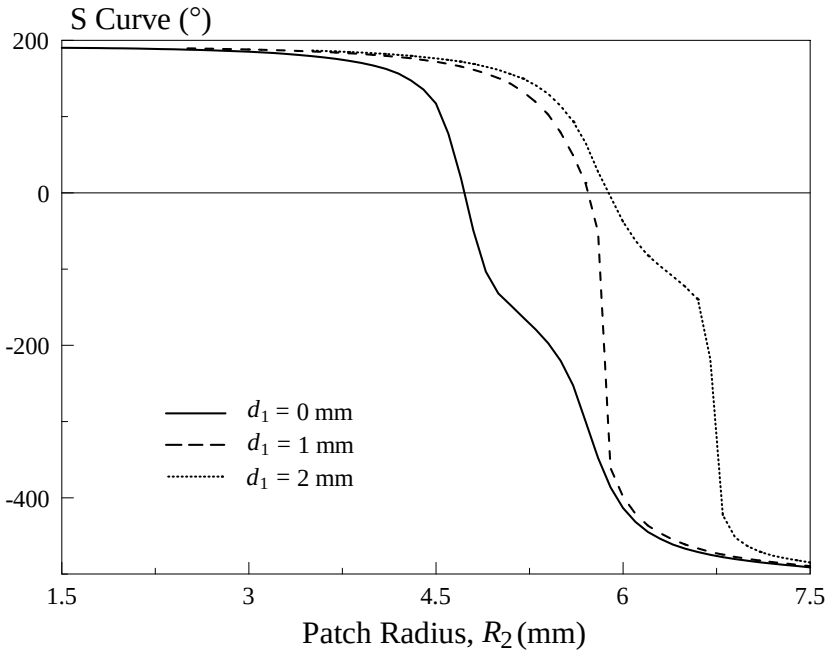

Figure 4.15: Effects of the Radius Difference d_1 (where $R_2 > R_1$) on the (a) Reflection Loss; (b) S Curve of the Proposed Double-Layered Reflectarray Unit Element.

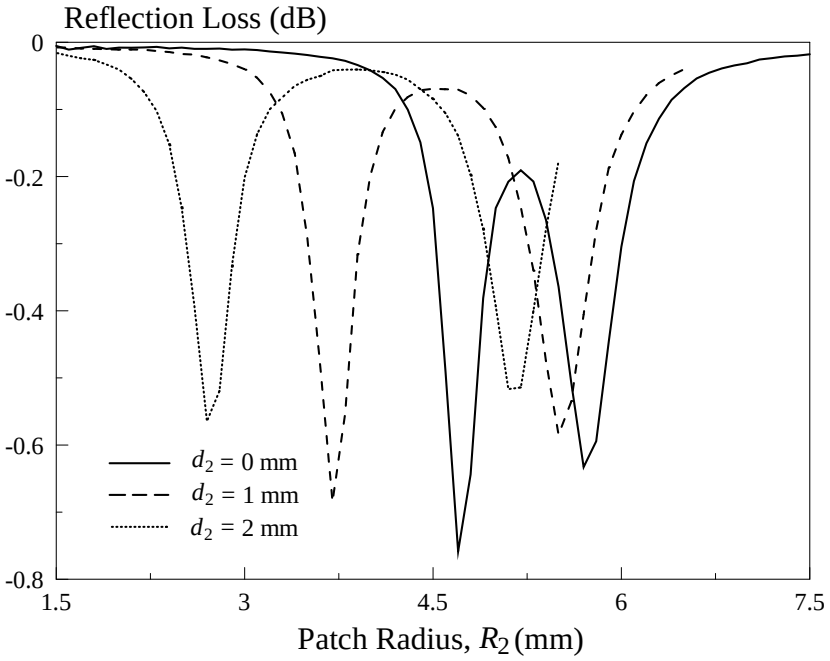

(a)

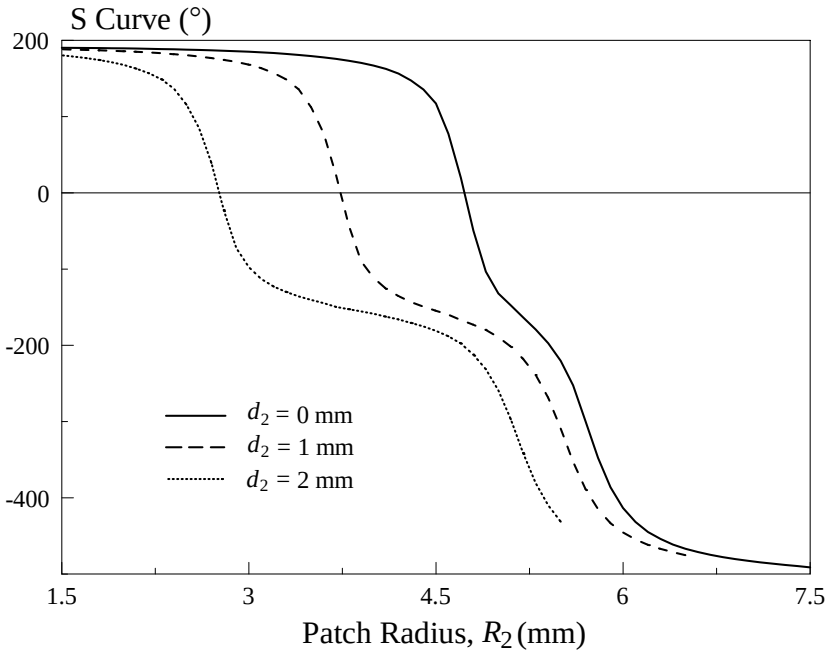

(b)

Figure 4.16: Effects of the Radius Difference d_2 (where $R_1 > R_2$) on the (a) Reflection Loss; (b) S Curve of the Proposed Double-Layered Reflectarray Unit Element.

4.5.4 Slot Inclination Angle

The cross-slotted top patch is rotated anticlockwise at four different angles (θ = 0°, 22.5°, 45° and 62.5°), with $R_1 = R_2$, to study the effect of the inclination angle on the reflection loss and S curve. With reference to Figure 4.17, it is obvious that rotating the top patch does not affect the performance of the reflection loss and S curve. For all four cases, they have the same reflection loss, reflection phase range, and slope.

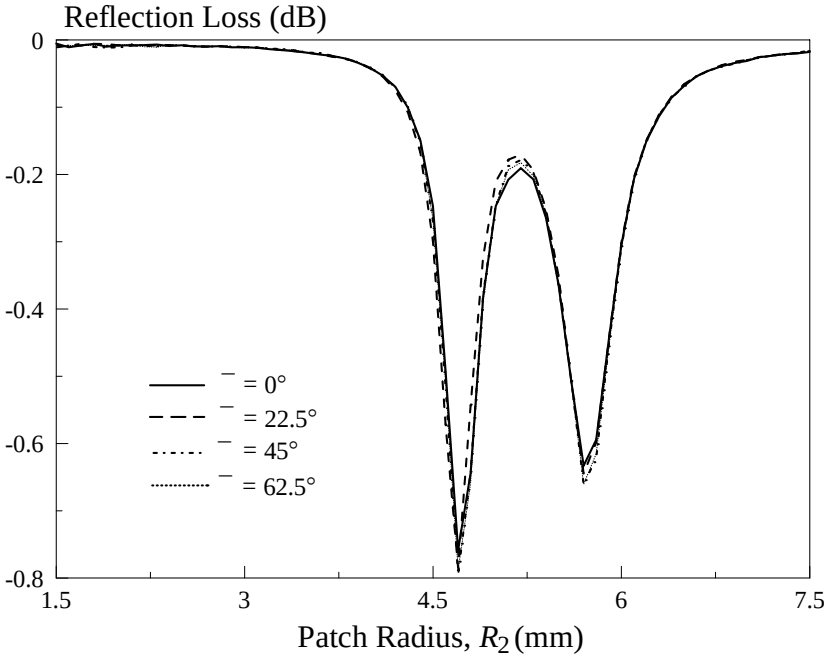

(a)

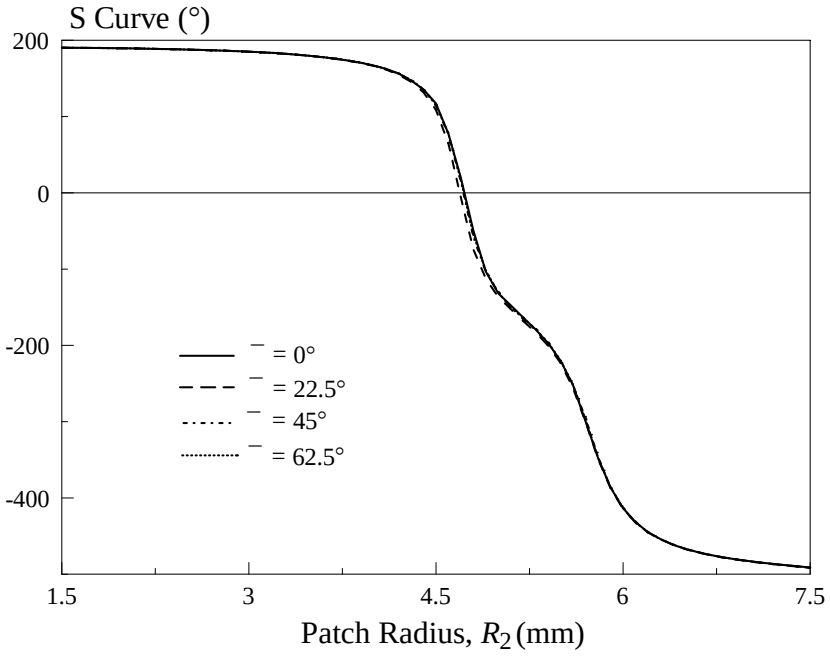

(b)

Figure 4.17: Effects of the Slot Inclination Angle θ on the (a) Reflection Loss; (b) S Curve of the Proposed Double-Layered Reflectarray Unit Element.

4.5.5 Substrates Thickness and Dielectric Constant

The thickness of the substrates (Substrate 1 and 2) is varied from 0.5 to 2.5 mm, with $R_1 = R_2$, and the reflection characteristics are analyzed. High reflection loss of ~ -22.5 dB is observed in Figure 4.18 (a) when substrates with a thickness of 2.5 mm are used. As can be seen from Figure 4.18 (b), the slope of the reflection phase becomes steeper with increasing substrates thickness. Substrates with thicknesses that can cause high reflection loss and rapid change of reflection phase slope should not be considered when designing the reflectarray.

To further study the effects of the substrates on the reflection characteristics, different sets of substrates (Substrate 1 and 2) with the same dielectric constant (ε_r) are simulated, with $R_1 = R_2$. Referring to Figure 4.19 (a), a slightly higher reflection loss which has a peak at -1.4 dB, when the patch radius R_2 = 4.1 mm, is observed if substrates with dielectric constant of 6.15 are used. The other two sets of substrates

(ε_r = 2 and 3.38) have a maximum reflection loss of ~ -0.7 dB, with both values close even though they are designed with different patch radii R_2. Again, it can be noted that using a substrate with higher dielectric constant (ε_r) value causes the unit element to resonate at a smaller patch radius of R_2. The reflection phase characteristics shown in Figure 4.19 (b) demonstrate that the slope gradient can be easily tuned without affecting the phase range.

Substrates (Substrate 1 and 2) with different loss tangents (tan δ) are also simulated to visualize their reflection characteristics. Again $R_1 = R_2$. With reference to Figure 4.20 (a), the reflection loss becomes higher with increasing loss tangent. With reference to Figure 4.20 (b), varying the loss tangent of the substrates does not affect the performance of the S curve.

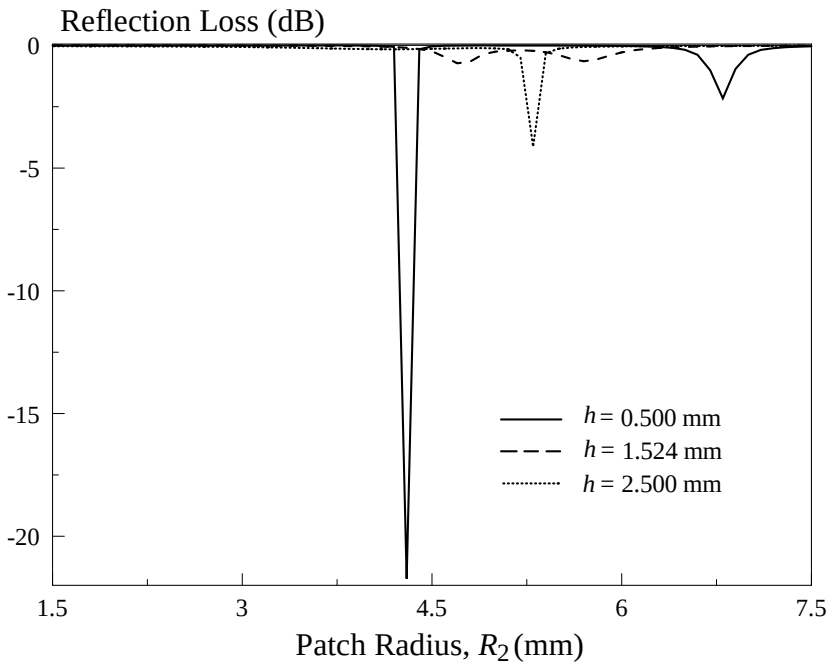

(a)

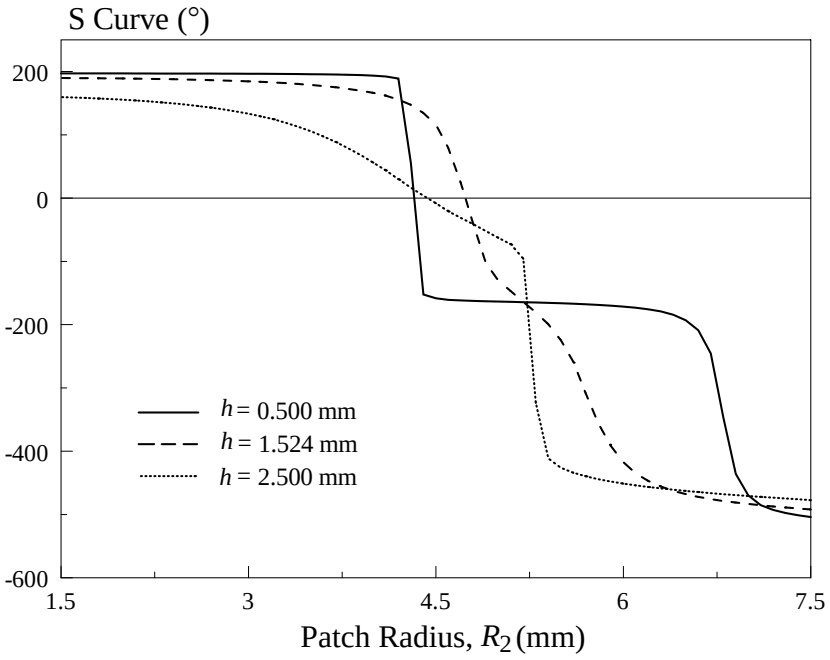

(b)

Figure 4.18: Effects of the Substrate Thickness *h* on the (a) Reflection Loss; (b) S Curve of the Proposed Double-Layered Reflectarray Unit Element.

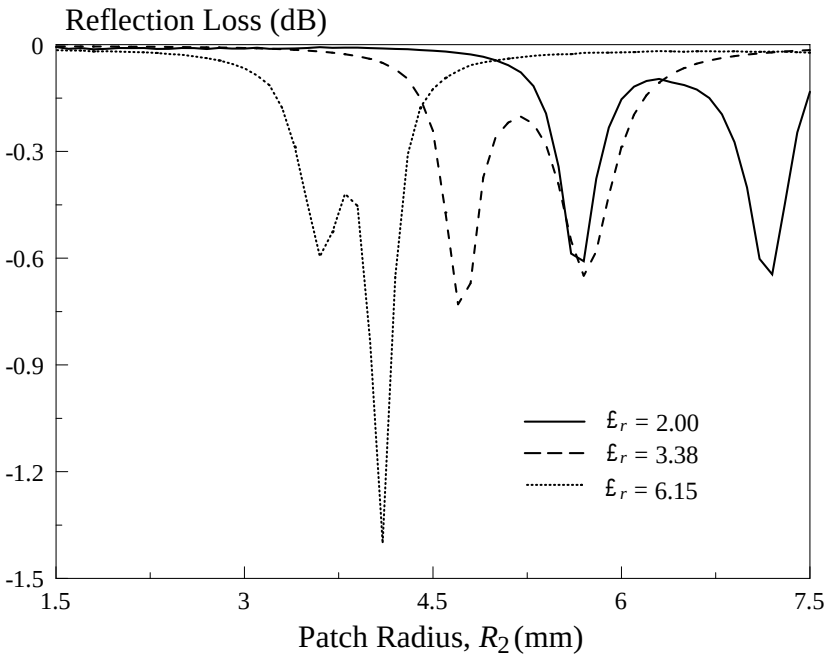

(a)

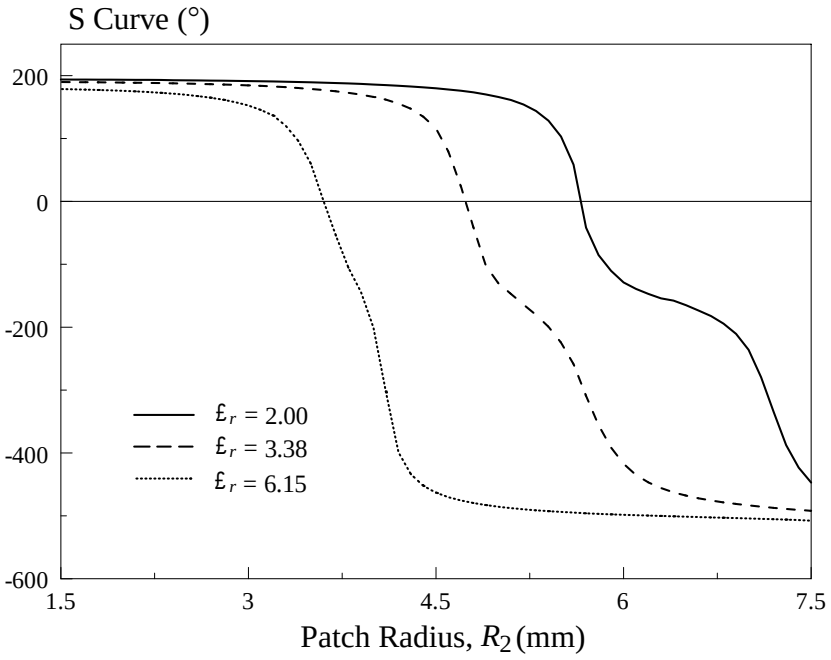

(b)

Figure 4.19: Effects of the Substrate Dielectric Constant ε_r on the (a) Reflection Loss; (b) S Curve of the Proposed Double-Layered Reflectarray Unit Element.

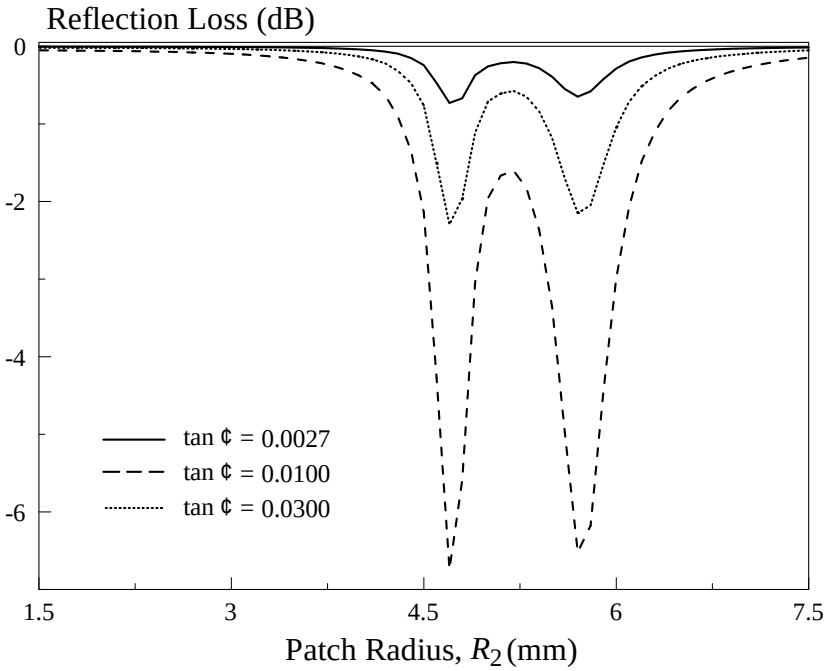

(a)

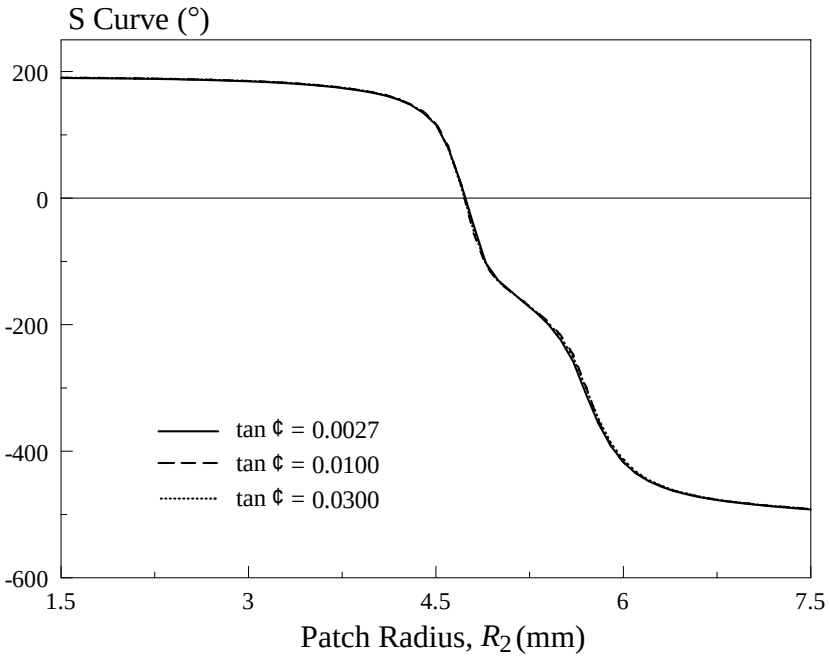

(b)

Figure 4.20: Effects of the Substrate Loss Tangent (tan *δ*) on the (a) Reflection Loss; (b) S Curve of the Proposed Double-Layered Reflectarray Unit Element.

4.5.6 Combinations of Top and Middle Circular Patches

In this section, unit elements with different combinations of top and middle circular patches are explored and their reflection characteristics are studied, shown in Figure 4.20. Referring to Figure 4.20 (a), the reflection loss for the unit element with either its top or middle patch etched with a pair of slots is shown to be able to be kept well below -1 dB. The unit element with both of its top and middle patches containing slots has the highest reflection loss, peaking at ~ -4.2 dB.

The S curve is then studied in Figure 4.20 (b). Comparing all of the four combinations of top and middle circular patches, unit element with only its top circular patch etched has the largest phase range with a reasonably slow reflection phase slope. Rapid change in gradient is observed for the unit element that has only its middle patch etched. This should be avoided when designing a reflectarray. Also,

it is noted that the unit element with slots etched on both patches is unable to provide a phase range of more than 400°, although a gradual phase slope is achievable.

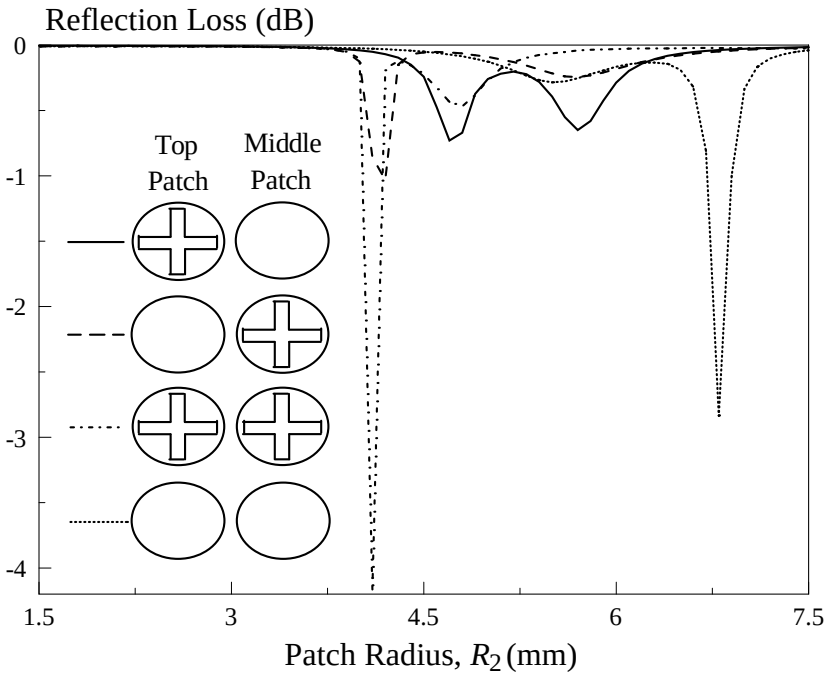

(a)

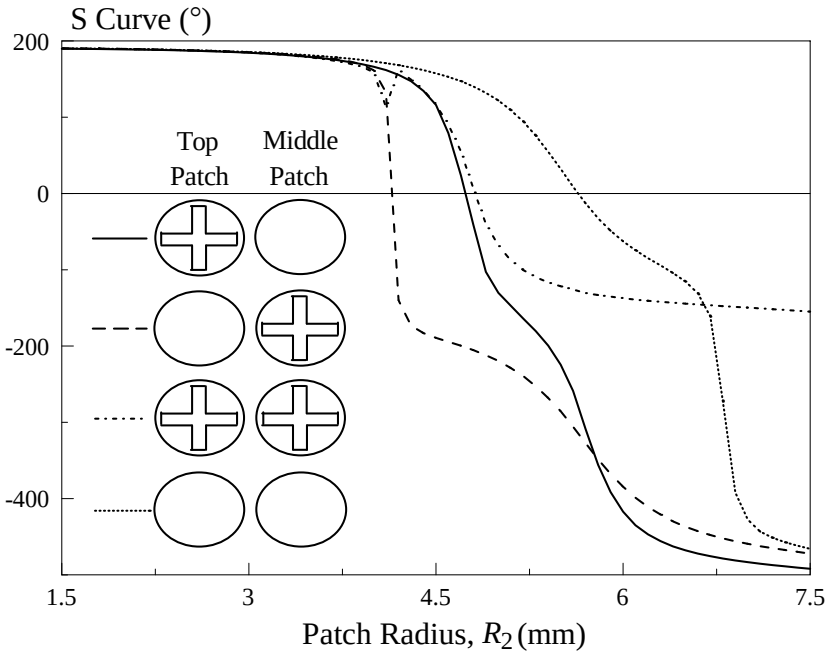

(b)

Figure 4.21: Effects of the Unit Elements with Different Combinations of Top and Middle Circular Patches on the (a) Reflection Loss; (b) S Curve of the Proposed Double-Layered Reflectarray Unit Element.

4.6 Conclusion

In this chapter, a double-layered microstrip reflectarray element with broad phase range has been proposed. A reflection phase range of 681.82° with low reflection loss (< -1 dB) is achievable. The effects of the patches, slots, and substrates of the unit element on the reflection characteristics have also been investigated. It has been found that the phase range can be manipulated by adjusting the radius of the middle circular patch. The changing rate of the reflection phase slope can be altered in several ways, namely, changing the slot widths simultaneously, adjusting the radius difference between two circular patches, and using substrates with different dielectric constants. It has also been found that the unit element with only its top circular patch etched is able to provide a very broad phase range with reasonably slow changing phase slope. Good agreement has been found between the simulated and experimental data.

CHAPTER 5

CONCLUSION AND RECOMMENDATIONS

Two novel microstrip-based reflectarray unit elements which operate at 6.5 GHz have been discussed in this dissertation. The configurations of the unit elements, along with the design procedures are presented. The prototypes are fabricated and measured using a vector network analyzer to verify the simulated results. Good agreement is found between simulation and measurement. In the first part, the single-layer cross-slotted circular microstrip unit element has been explored. Varying the two slot lengths at the same time is proven to be able to introduce phase shifts to the S curve. In the second part, the double-layer circular microstrip reflectarray element has been proposed. It was shown that the unit element can provide a broad phase range of 681.82°. It has also been found that the phase range can be manipulated by adjusting the radius of the middle circular patch.

The two novel unit elements can be further utilized to design reflectarrays for future development. The single-layer cross-slotted circular patch unit element is sufficient for designing small-size reflectarrays. Since the proposed double-layer circular microstrip unit element has achieved a large phase range of much larger than 360°, it can be used to design reflectarrays with any sizes.

REFERENCES

Abd-Elhady, M. and Hong, W., 2010. Ka-band linear polarized air vias reflectarray. *IEEE Middle East Conference on Antennas and Propagation*, pp.1–3.

Abd-Elhady, M., Hong, W. and Zhang, Y., 2012. A Ka-band reflectarray implemented with a single-layer perforated dielectric substrate. *IEEE Antennas and Wireless Propagation Letters*, 11, pp.600–603.

Berry, D., Malech, R. and Kennedy, W., 1963. The reflectarray antenna. *IEEE Transactions on Antennas and Propagation*, 11(6), pp.645–651.

Bialkowski, M.E. and Sayidmarie, K.H., 2008. Investigations into phase characteristics of a single-Layer reflectarray employing patch or ring elements of variable size. *IEEE Transactions on Antennas and Propagation*, 56(11), pp.3366–3372.

Bozzi, M., Germani, S. and Perregrini, L., 2004. A figure of merit for losses in printed reflectarray elements. *IEEE Antennas and Wireless Propagation Letters*, 3(1), pp.257–260.

Budhu, J. and Rahmat-Samii, Y., 2011. Understanding the appearance of specular reflection in offset fed reflectarray antennas. *IEEE International Symposium on Antennas and Propagation*, pp.97–100.

Cadoret, D., Laisné, A., Gillard, R. and Legay, H., 2005. A new reflectarray cell using microstrip patches loaded with slots. *Microwave and Optical Technology Letters*, 44(3), pp.270–272.

Capozzoli, A., Curcio, C., D'Elia, G., Liseno, A., Bresciani, D. and Legay, H., 2009. Fast phase-only synthesis of faceted reflectarrays. *European Conference on Antennas and Propagation*, pp.1329–1333.

Carrasco, E., Arrebola, M. and Encinar, J.A., 2007. Shaped beam reflectarray using aperture-coupled delay lines for LMDS central station. *The Second European Conference on Antennas and Propagation*, pp.1–6.

Carrasco, E., Arrebola, M., Encinar, J.A. and Barba, M., 2008. Demonstration of a shaped beam reflectarray using aperture-coupled delay lines for LMDS central

station antenna. *IEEE Transactions on Antennas and Propagation*, 56(10), pp.3103–3111.

Chaharmir, M.R., Shaker, J., Cuhaci, M. and Ittipiboon, A., 2006. A broadband reflectarray antenna with double square rings. *Microwave and Optical Technology Letters*, 48(7), pp.1317–1320.

Chaharmir, M.R., Shaker, J., Cuhaci, M. and Sebak, A., 2003. Reflectarray with variable slots on ground plane. *IEE Proceedings Microwaves, Antennas and Propagation*, 150(6), p.436.

Chaharmir, M.R., Shaker, J., Gagnon, N. and Lee, D., 2010. Design of broadband, single layer dual-band large reflectarray using multi open loop elements. *IEEE Transactions on Antennas and Propagation*, 58(9), pp.2875–2883.

Chang, D.-C. and Huang, M.-C., 1995. Multiple-polarization microstrip reflectarray antenna with high efficiency and low cross-polarization. *IEEE Transactions on Antennas and Propagation*, 43(8), pp.829–834.

Dzulkipli, I., Jamaluddin, M.H., Gillard, R., Sauleau, R., Ngah, R., Kamarudin, M.R., Seman, N. and Rahim, M.K.A., 2012. Mutual coupling analysis using FDTD for dielectric resonator antenna reflectarray radiation prediction. *Progress In Electromagnetics Research B*, 41, pp.121–136.

Encinar, J.A., 1999. Design of two-layer printed reflectarrays for bandwidth enhancement. *IEEE Antennas and Propagation Society International Symposium*, 2, pp.1164–1167.

Encinar, J.A., 2001. Design of two-layer printed reflectarrays using patches of variable size. *IEEE Transactions on Antennas and Propagation*, 49(10), pp.1403–1410.

Encinar, J.A., Arrebola, M., Fuente, L.F. and Toso, G., 2011. A transmit-receive reflectarray antenna for direct broadcast satellite applications. *IEEE Transactions on Antennas and Propagation*, 59(9), pp.3255–3264.

Encinar, J.A. and Zornoza, J.A., 2003. Broadband design of three-layer printed reflectarrays. *IEEE Transactions on Antennas and Propagation*, 51(7), pp.1662–1664.

Encinar, J.A. and Zornoza, J.A., 2004. Three-layer printed reflectarrays for contoured beam space applications. *IEEE Transactions on Antennas and Propagation*, 52(5), pp.1138–1148.

Guo, Y.J. and Barton, S.K., 1995. Phase correcting zonal reflector incorporating rings. *IEEE Transactions on Antennas and Propagation*, 43(4), pp.350–355.

Han, C., Huang, J. and Chang, K., 2006. Cassegrain offset subreflector-fed X/Ka dual-band reflectarray with thin membranes. *IEEE Transactions on Antennas and Propagation*, 54(10), pp.2838–2844.

Hasani, H., Kamyab, M. and Mirkamali, A., 2010. Broadband reflectarray antenna incorporating disk elements with attached phase-delay lines. *IEEE Antennas and Wireless Propagation Letters*, 9, pp.156–158.

Huang, J., 1991. Microstrip reflectarray. *Antennas and Propagation Society Symposium*, 2, pp.612–615.

Huang, J., 1995. Analysis of a microstrip reflectarray antenna for microspacecraft applications. *TDA Progress Report 42-120*, pp.153–173.

Huang, J., 1996. Capabilities of printed reflectarray antennas. *IEEE International Symposium on Phased Array Systems and Technology*, pp.131–134.

Huang, J. and Encinar, J.A., 2007. *Reflectarray antennas*. Hoboken, NJ: John Wiley & Sons.

Karnati, K.K., Yusuf, Y., Ebadi, S. and Gong, X., 2013. Theoretical analysis on reflection properties of reflectarray unit cells using quality factors. *IEEE Transactions on Antennas and Propagation*, 61(1), pp.201–210.

Khor, Y.C., Lim, E.H. and Chung, B.K., 2014. Broadside-coupled filtering circular patch power dividers. *Progress In Electromagnetics Research C*, 48, pp.1–9.

Li, Y., Bialkowski, M.E., Sayidmarie, K.H. and Shuley, N.V., 2010. Microstrip reflectarray formed by double elliptical ring elements. *Proceedings of the Fourth European Conference on Antennas and Propagation*, pp.1–5.

Maddahali, M. and Forooraghi, K., 2013. High efficiency reflectarray using smooth tapering in phase pattern on antenna surface. *Microwave and Optical Technology Letters*, 55(4), pp.747–753.

Malagisi, C.S., 1978. Microstrip disc element reflect array. *Electronics and Aerospace Systems Convention*, pp.186–192.

Maruyama, T., Furuno, T., Oda, Y., Shen, J. and Ohya, T., 2010a. Analysis and design of metamaterial reflectarray using combination of multilayer mushroom-structure. *IEEE Antennas and Propagation Society International Symposium*, pp.1–4.

Maruyama, T., Furuno, T., Oda, Y., Shen, J. and Ohya, T., 2010b. Capacitance value control for metamaterial reflectarray using multi layer mushroom-structure with parasitic element. *IEEE International Conference on Wireless Information Technology and Systems*, pp.1–4.

Maruyama, T., Furuno, T., Oda, Y., Shen, J., Tran, N. and Kayama, H., 2011. Design of wide angle reflection reflectarray using multi-layer mushroom structure to improve propagation. *XXXth URSI General Assembly and Scientific Symposium*, pp.1–4.

Mener, S., Gillard, R., Sauleau, R., Cheymol, C. and Potier, P., 2013. Design and characterization of a CPSS-based unit-cell for circularly polarized reflectarray applications. *IEEE Transactions on Antennas and Propagation*, 61(4), pp.2313–2318.

Mussetta, M., Pirinoli, P., Bliznyuk, N., Engheta, N. and Zich, R.E., 2006. Frequency response of a gangbuster surface off-set reflectarray antenna. *IEEE Antennas and Propagation Society International Symposium*, pp.4327–4330.

Mussetta, M., Zhang, W.X., Wang, A.N., Chen, H.H. and Zich, R.E., 2007. Frequency response optimization of a double layer reflectarray antenna. *IEEE Antennas and Propagation International Symposium*, pp.5319–5322.

Pan, Y., Zhang, Y. and Karimkashi, S., 2012. Broadband low-cost reflectarray for multi-mission radar applications. *IEEE Radar Conference*, pp.0613–0617.

Pham, K.T., Nguyen, B.D., Bui, L.-P.P., Tran, V.-S. and Mai, L., 2012. Reflectarray element based on variable line length for millimeter-wave radar applications. *International Conference on Advanced Technologies for Communications*, pp.218–221.

Phelan, H.R., 1977. Spiraphase reflectarray for multitarget radar. *Microwave Journal*, 20, pp.67–73.

Pozar, D.M. and Metzler, T.A., 1993. Analysis of a reflectarray antenna using microstrip patches of variable size. *Electronics Letters*, 29(8), p.657.

Pozar, D.M., Targonski, S.D. and Pokuls, R., 1999. A shaped-beam microstrip patch reflectarray. *IEEE Transactions on Antennas and Propagation*, 47(7), pp.1167–1173.

Pozar, D.M., Targonski, S.D. and Syrigos, H.D., 1997. Design of millimeter wave microstrip reflectarrays. *IEEE Transactions on Antennas and Propagation*, 45(2), pp.287–296.

Rajagopalan, H. and Rahmat-Samii, Y., 2010. On the reflection characteristics of a reflectarray element with low-loss and high-loss substrates. *IEEE Antennas and Propagation Magazine*, 52(4), pp.73–89.

Robinson, A.W. and Bialkowski, M.E., 1997. An X-band active microstrip reflectarray. *Asia-Pacific Microwave Conference Proceedings*, 3, pp.925–928.

Trampuz, C., Hajian, M. and Ligthart, L., 2006. Design, analysis and measurements of reflected phased array microstrip antennas at ka-band, using hollow phasing. *European Radar Conference*, pp.57–60.

Watkins, J., 1969. Circular resonant structures in microstrip. *Electronics Letters*, 5(21), pp.524–525.

Yang, F., Kim, Y., Yu, A., Huang, J. and Elsherbeni, A., 2007. A single layer reflectarray antenna for C/X/Ka bands applications. *International Conference on Electromagnetics in Advanced Applications*, pp.1058–1061.

Yu, A., Yang, F., Elsherbeni, A.Z. and Huang, J., 2009. Design and measurement of a circularly polarized Ka-band reflectarray antenna. *European Conference on Antennas and Propagation*, pp.2769–2773.

Zhang, W.-X., Fu, D.-L. and Wang, A.-N., 2007. A compound printed air-fed array antenna. *International Conference on Electromagnetics in Advanced Applications*, pp.1054–1057.

Zhao, M.-Y., Zhang, G.-Q., Lei, X., Wu, J.-M. and Shang, J.-Y., 2013. Design of new single-layer multiple-resonance broadband circularly polarized reflectarrays. *IEEE Antennas and Wireless Propagation Letters*, 12, pp.356–359.

Zhou Danchen, Niu Zhenyi and Li Ruilin, 2011. Investigation on a single-layer microstrip circular-patch/ring-combination reflectarray element. *Cross Strait Quad-Regional Radio Science and Wireless Technology Conference*, 1, pp.664–667.

Zhou, M., Sorensen, S.B., Kim, O.S., Jorgensen, E., Meincke, P. and Breinbjerg, O., 2013. Direct optimization of printed reflectarrays for contoured beam satellite antenna applications. *IEEE Transactions on Antennas and Propagation*, 61(4), pp.1995–2004.

Zubir, F. and Rahim, M.K.A., 2009. Simulated fractals shape for unit cell reflectarray. *Asia Pacific Microwave Conference*, pp.583–586.